

# Backstepping Neural Operators for $2 \times 2$ Hyperbolic PDEs

Shanshan Wang<sup>a</sup>, Mamadou Diagne\*<sup>b</sup>, Miroslav Krstic<sup>b</sup>

<sup>a</sup>Department of Control Science and Engineering, University of Shanghai for Science and Technology, Shanghai, P. R. China, 200093

<sup>b</sup>Department of Mechanical and Aerospace Engineering, University of California San Diego, La Jolla, CA, USA, 92093

---

## Abstract

Deep neural network approximation of nonlinear operators, commonly referred to as DeepONet, has proven capable of approximating PDE backstepping designs in which a single Goursat-form PDE governs a single feedback gain function. In boundary control of coupled PDEs, coupled Goursat-form PDEs govern two or more gain kernels—a PDE structure unaddressed thus far with DeepONet. In this paper, we explore the subject of approximating systems of gain kernel PDEs for hyperbolic PDE plants by considering a simple counter-convecting  $2 \times 2$  coupled system in whose control a  $2 \times 2$  kernel PDE system in Goursat form arises. Engineering applications include oil drilling, the Saint-Venant model of shallow water waves, and the Aw-Rascle-Zhang model of stop-and-go instability in congested traffic flow. We establish the continuity of the mapping from a total of five plant PDE functional coefficients to the kernel PDE solutions, prove the existence of an arbitrarily close DeepONet approximation to the kernel PDEs, and ensure that the DeepONet-approximated gains guarantee stabilization when replacing the exact backstepping gain kernels. Taking into account anti-collocated boundary actuation and sensing, our  $L^2$ -Globally-exponentially stabilizing (GES) approximate gain kernel-based output feedback design implies the deep learning of both the controller's and the observer's gains. Moreover, the encoding of the output-feedback law into DeepONet ensures *semi-global practical exponential stability (SG-PES)*. The DeepONet operator speeds up the computation of the controller gains by multiple orders of magnitude. Its theoretically proven stabilizing capability is demonstrated through simulations.

*Key words:* PDE backstepping, deep learning, neural networks, distributed parameter systems

---

## 1 Introduction

The versatility of coupled first-order hyperbolic PDE systems across various fields extends to applications such as modeling traffic dynamics [1, 2], open channel fluid flow [3–6], heat exchanger systems [7], oil drilling operations [8], flexible pipe assemblies [9], natural gas pipeline networks [10], and power transmission line networks [11], among others.

### 1.1 Control of coupled linear hyperbolic PDE systems

The development of stabilizing boundary feedback laws for counter-convective first-order linear hyperbolic systems has evolved since the introduction of the locally exponentially stabilizing boundary controller in [12]. This controller was originally crafted for the Saint-Venant model, a nonlinear coupled hyperbolic PDE. Importantly, assuming some compatibility condition of the initial data and restricting the set of admissible equilibrium, [12] introduced the simplest entropy-based Lyapunov function to control a system whose total energy is not a suitable Lyapunov candidate. After [12],

the Riemann invariants method enabled the determination of gate operating conditions that ensure exponential stability relying exclusively on local water level measurements at the gate positions, in the absence of friction. Adaptive backstepping control of a wave PDE with anti-damping represented in Riemann variables as a coupled first-order hyperbolic PDE was developed in [13]. Fundamental contributions, [14, 15], along with [16], have led to the formulation of a quadratic Lyapunov candidate for  $2 \times 2$  linear hyperbolic systems. Our work revolves around the PDE backstepping approach, which relies on a single boundary actuation and a full-state measurement, as outlined in the reference [16]. The approach described in [14, 15] could be referred to as the “dissipativity” method as it pertains to finding dissipative boundary conditions that are similar to “small gain conditions.” Furthermore, results in [14, 15] are based on a dual boundary actuation strategy. They exclusively leverage measurements obtained from the boundary positions, so to speak, at the gate locations of a water canal to achieve stabilization. Results on bilateral or dual boundary control of hyperbolic PDEs by means of PDE backstepping were reported in [17, 18]. Delay-adaptive boundary control of coupled hyperbolic PDE-ODE cascade systems was recently established in [19] via Batch-Least Square Identification (BaLSI) [20]. Alongside these two major ap-

---

\* Corresponding author: Mamadou Diagne.

Email addresses: wss\_dhu@126.com (Shanshan Wang), mdiagne@ucsd.edu (Mamadou Diagne\*), krstic@ucsd.edu (Miroslav Krstic).

proaches, a range of methods, including frequency domain analysis [21], differential flatness [22], sliding-mode control [23], and proportional-integral control [24], have been employed for the design of control laws for  $2 \times 2$  hyperbolic system of balance laws.

Aiming at stabilizing a two-phase slugging phenomenon observed in oil drilling processes [25], PDE backstepping has been used to control a  $2 + 1$  counter-convective system actuated at one boundary [26]. The problem structure outlined in [25] has broad applicability, appearing in various multiphase flow processes like drift-flux modeling in oil drilling [27] and coupled water-sediment dynamics in river breaches [4]. In the latter case, the backstepping method achieves exponential stabilization of supercritical flow regimes, which was not attainable by the design proposed in [26]. A similar system's structure, but in the  $3 + 1$  form, can be found in [28], where the control of a two-class traffic system is studied.

Generalized results on the exponential stabilization of an arbitrary number of coupled waves among which a single pattern is controlled were achieved in [29]. It is a non-trivial extension of the backstepping approach [16, 26] to the so-called  $n + 1$  case where the boundary actuation of a single counter-convective pattern regulates systems with an arbitrary number of coupled waves. Later on, systems consisting of  $n + m$  coupled linear hyperbolic PDE systems were exponentially stabilized by actuating  $m$  components in [30] (see [31] for the inhomogeneous quasilinear case), and stability in minimum time was provided in [32]. Following these major developments, [33] proposed an adaptive observer to estimate the boundary parameters of an  $n + 1$  system motivated by the need to identify the bottom hole influxes of hydrocarbon caused by high pressure formations in the well during oil drilling operations. The extension of [33] to  $n + m$  systems in [34] was followed by major progress on adaptive control design [35]. The recent results in [36, 37] allow for finite-time stabilization of linear and coupled hyperbolic systems with space and time-dependent parameters. In light of the current context, it's worth noting the emergence of nonlinear controllers for nonlinear infinite-dimension systems of conservation laws [38, 39]. These controllers demonstrate the potential for achieving global exponential stabilization of spill-free transfer systems governed by nonlinear and coupled hyperbolic systems.

In general, the conception of PDE controllers can lead to complex gain functions that require non-obvious computational effort. Our contribution signifies an advancement in leveraging the computational capabilities offered by machine learning techniques to enhance the feasibility of hyperbolic PDE control.

## 1.2 Contributions

We expedite the computation of gain kernel PDEs that emerge from backstepping design for coupled linear hyperbolic systems. Developing further the DeepONet design originally introduced in [40] and then [41, 42] for simpler PDE systems, we introduce Neural Operator (NO) approximations for kernels applicable to  $2 \times 2$  hyperbolic PDEs to encapsulate the mapping from the functional coefficients

of the plant into a previously trained DeepONet. We design a neural network architecture, or more precisely, a computational resource capable of calculating the gains through function evaluations, eliminating the necessity to solve the coupled gain kernel PDEs defined on a triangular domain. Recently, DeepONet achieved gain kernel computation for full-state feedback control in the ARZ traffic system (simpler case) in [43]. Furthermore, results on DeepONet-based adaptive control [44], gain scheduling [45], and moving-horizon estimators (MHE) [46] were recently developed.

Differing from [47], where DeepONet approximation of gain kernel PDEs was achieved using a composition of operators defined by a single hyperbolic PDE in Goursat form and one parabolic PDE on a rectangular domain, the scenario involving coupled hyperbolic PDEs in cascade, along with their state observer, gives rise to an approximate closed-loop system governed by four interconnected Goursat-form PDEs. Two of these Goursat-form PDEs originate from the controller, and the remaining two characterize the gain function of the observer. Both the DeepONet approximates of the controller and the observer gain functions are the output of the  $2 \times 2$  coupled nonlinear operators of Goursat PDEs fed by a total of five plant functional coefficients. The configuration of the studied DeepONet-approximate nonlinear operators expands the scope of NO designs originally introduced by the Machine Learning community [48–51] because such a distinctive coupling between Goursat PDEs is primarily established through backstepping control design. Our present contribution is twofold:

- **DeepONet for the gain kernels of the output-feedback law.** We derive a *Global Exponential Stability (GES)* result for a  $2 \times 2$  linear hyperbolic PDE system equipped with an output feedback control law fed by the NO-approximate controller's and observer's gain functions. Considering that the controller-observer system is a composition of two linear systems, the global exponential stability of the closed-loop system that is achieved by the exact gain functions is preserved under the approximated one with an estimate of the decay rate. The effect of the accuracy of the approximation on the convergence rate is elucidated: less accurate data slows the decay rate.
- **Encoding of the output feedback law.** Utilizing insights gained from the DeepONet controller and observer gain kernels, as well as the observed system state values, we develop a neural operator (NO) approximation for the output-feedback control law, including the state of the observer. This case deals with the complete learning of a control law for a  $2 \times 2$  linear and coupled hyperbolic system using anti-collocated boundary actuation and sensing. We establish a *Semi-global Practical Exponential Stability (SG-PES)* estimate for the resulting closed-loop system. The SG-PES result cannot be attributed to the approximation of Goursat-form PDEs that are multiplicative gain kernels embedded within the control law and the state estimator, but to the approximation of the observer states  $u$  and  $v$  that are also used into a *fully-learned* control law. As stated concisely, the approximation error is not solely multiplicative but also additive, resulting in the SG-PES outcome. In a nutshell, the stability result is semi-global

considering that the dataset includes samples of observer states  $u$  and  $v$  with bounded magnitudes.

In both cases, the method accelerates the computation of control gains, significantly improving computation speed. Our theoretically proven stability result is demonstrated through simulations, and the code is available on github.

**Organization of paper:** Section 2 succinctly presents the design of an exponentially stabilizing output-feedback boundary control law for  $2 \times 2$  hyperbolic PDE systems. Sections 3 and 4 present the approximation of the kernel operators and the global exponential stabilization (GES) under the approximated controller's gain functions and observer's gain functions via DeepONet. Section 5 presents a semi-global practical exponential stability (SG-PES) result when the totality of the output feedback law is learned via DeepONet. Section 6 and Section 7 present our simulation results and concluding remarks, respectively.

**Notation:** We define the  $L^2$ -norm for  $\chi(x) \in L^2[0, 1]$  as  $\|\chi\|_{L^2}^2 = \int_0^1 |\chi(x)|^2 dx$ . For the convenience, we set  $\|\chi\|^2 = \|\chi\|_{L^2}^2$ . The supremum norm is denoted  $\|\cdot\|_\infty$ .

## 2 Preliminaries and problem statement

**Preliminaries.** We consider linear hyperbolic systems

$$\partial_t u(x, t) = -\lambda(x)\partial_x u(x, t) + \sigma(x)u(x, t) + \omega(x)v(x, t), \quad (1)$$

$$\partial_t v(x, t) = \mu(x)\partial_x v(x, t) + \theta(x)u(x, t), \quad (2)$$

with boundary conditions

$$u(0, t) = qv(0, t), \quad (3)$$

$$v(1, t) = U(t), \quad (4)$$

where,

$$\lambda, \mu \in C^1([0, 1]), \quad (5)$$

$$\sigma, \omega, \theta \in C^0([0, 1]), \quad (6)$$

$$q \in \mathbb{R}, \quad (7)$$

and initial conditions

$$v^0(x), u^0(x) \in L^2([0, 1]). \quad (8)$$

The transport speeds are assumed to satisfy

$$-\mu(x) < 0 < \lambda(x), \quad \forall x \in [0, 1], \quad (9)$$

and  $\lambda, \mu, \sigma, \omega, \theta$  are all bounded with  $\underline{\lambda} \leq \lambda \leq \bar{\lambda}, \underline{\mu} \leq \mu \leq \bar{\mu}, \underline{\sigma} \leq \sigma \leq \bar{\sigma}, \underline{\omega} \leq \omega \leq \bar{\omega}$ , and  $\underline{\theta} \leq \theta \leq \bar{\theta}$ .

### 2.1 Full-state boundary feedback control law

Exploiting the following backstepping transformation [29],

$$\begin{aligned} \beta(x, t) &= v(x, t) - \int_0^x k_1(x, \xi)u(\xi, t)d\xi \\ &\quad - \int_0^x k_2(x, \xi)v(\xi, t)d\xi, \end{aligned} \quad (10)$$

system (1)–(4) can be transformed into the target system

$$\partial_t u(x, t) = -\lambda(x)\partial_x u(x, t) + \sigma(x)u(x, t) + \omega(x)\beta(x, t)$$

$$+ \int_0^x c(x, \xi)u(\xi, t)d\xi + \int_0^x \kappa(x, \xi)\beta(\xi, t)d\xi, \quad (11)$$

$$\partial_t \beta(x, t) = \mu(x)\partial_x \beta(x, t), \quad (12)$$

with boundary conditions defined as

$$u(0, t) = q\beta(0, t), \quad (13)$$

$$\beta(1, t) = 0, \quad (14)$$

where  $c(x, \xi)$  and  $\kappa(x, \xi)$  are functions to be determined. The realization of this mapping requires the kernels in the backstepping transformation (10) to satisfy the following PDEs<sup>1</sup>

$$\mu(x)\partial_x k_1 - \lambda(\xi)\partial_\xi k_1 = \lambda'(\xi)k_1 + \sigma(\xi)k_1 + \theta(\xi)k_2, \quad (15)$$

$$\mu(x)\partial_x k_2 + \mu(\xi)\partial_\xi k_2 = -\mu'(\xi)k_2 + \omega(\xi)k_1, \quad (16)$$

with boundary conditions

$$k_1(x, x) = -\frac{\theta(x)}{\lambda(x) + \mu(x)}, \quad (17)$$

$$\mu(0)k_2(x, 0) = q\lambda(0)k_1(x, 0). \quad (18)$$

The system (15)–(18) defined over the triangular domain  $\mathcal{T} = \{(x, \xi) \mid 0 \leq \xi \leq x \leq 1\}$ , is a coupled  $2 \times 2$  Goursat-form PDEs govern two gain kernels and the coefficient  $\kappa$  and  $c$  are chosen to satisfy

$$\kappa(x, \xi) = \omega(x)k_2(x, \xi) + \int_\xi^x \kappa(x, s)k_2(s, \xi)ds, \quad (19)$$

$$c(x, \xi) = \omega(x)k_1(x, \xi) + \int_\xi^x \kappa(x, s)k_1(s, \xi)ds. \quad (20)$$

From (4), (10), and (14), the boundary controller is

$$U(t) = \int_0^1 k_1(1, \xi)u(\xi, t)d\xi + \int_0^1 k_2(1, \xi)v(\xi, t)d\xi. \quad (21)$$

The invertibility of the transformation (10) together with the existence of unique solution to (15)–(18) is established in [29]. The invertibility of the transformation induces equivalent stability properties of the target and original systems.

The inverse transformation of (10) is given by

$$\begin{aligned} v(x, t) &= \beta(x, t) + \int_0^x l_1(x, \xi)u(\xi, t)d\xi \\ &\quad + \int_0^x l_2(x, \xi)\beta(\xi, t)d\xi, \end{aligned} \quad (22)$$

where

$$l_1(x, \xi) = k_1(x, \xi) + \int_\xi^x k_2(x, s)l_1(s, \xi)ds, \quad (23)$$

$$l_2(x, \xi) = k_2(x, \xi) + \int_\xi^x k_2(x, s)l_2(s, \xi)ds. \quad (24)$$

### 2.2 Observer design for an output feedback control law

Our goal is to develop an exponentially convergent observer capable of estimating the spatially distributed states of system (1)–(4) using the available boundary point mea-

<sup>1</sup> Here, we use the prime notation to indicate derivatives.

surement  $v(0,t)$ , which is anti-collocated with the boundary point of actuation. We design an observer consisting of the copy of the plant plus some output injection terms. The derivation of the observer's gains that ensure convergence of the estimated states to the plant states is completed using backstepping design. The following observer is stated:

$$\begin{aligned} \partial_t \hat{u}(x,t) = & -\lambda(x)\partial_x \hat{u}(x,t) + \sigma(x)\hat{u}(x,t) + \omega(x)\hat{v}(x,t) \\ & + p_1(x)(v(0,t) - \hat{v}(0,t)), \end{aligned} \quad (25)$$

$$\begin{aligned} \partial_t \hat{v}(x,t) = & \mu(x)\partial_x \hat{v}(x,t) + \theta(x)\hat{u}(x,t) \\ & + p_2(x)(v(0,t) - \hat{v}(0,t)), \end{aligned} \quad (26)$$

with boundary conditions

$$\hat{u}(0,t) = qv(0,t), \quad (27)$$

$$\hat{v}(1,t) = U(t). \quad (28)$$

The functions  $p_1(x)$  and  $p_2(x)$  are the observer output injection gains to be determined via backstepping design. Denoting the observer error

$$\tilde{u}(x,t) = u(x,t) - \hat{u}(x,t), \quad (29)$$

$$\tilde{v}(x,t) = v(x,t) - \hat{v}(x,t), \quad (30)$$

it follows the error dynamics

$$\begin{aligned} \partial_t \tilde{u}(x,t) = & -\lambda(x)\partial_x \tilde{u}(x,t) + \sigma(x)\tilde{u}(x,t) \\ & + \omega(x)\tilde{v}(x,t) - p_1(x)\tilde{v}(0,t), \end{aligned} \quad (31)$$

$$\begin{aligned} \partial_t \tilde{v}(x,t) = & \mu(x)\partial_x \tilde{v}(x,t) + \theta(x)\tilde{u}(x,t) - p_2(x)\tilde{v}(0,t), \end{aligned} \quad (32)$$

with boundary conditions

$$\tilde{u}(0,t) = 0, \quad (33)$$

$$\tilde{v}(1,t) = 0. \quad (34)$$

To design the observer output injection gains, backstepping transformations are again introduced as

$$\tilde{u}(x,t) = \tilde{\alpha}(x,t) + \int_0^x m_1(x,\xi)\tilde{\beta}(\xi,t)d\xi, \quad (35)$$

$$\tilde{v}(x,t) = \tilde{\beta}(x,t) + \int_0^x m_2(x,\xi)\tilde{\beta}(\xi,t)d\xi, \quad (36)$$

to map system (31)–(34) into the target system

$$\begin{aligned} \partial_t \tilde{\alpha}(x,t) = & -\lambda(x)\partial_x \tilde{\alpha}(x,t) + \sigma(x)\tilde{\alpha}(x,t) \\ & + \int_0^x g(x,\xi)\tilde{\alpha}(\xi,t)d\xi, \end{aligned} \quad (37)$$

$$\begin{aligned} \partial_t \tilde{\beta}(x,t) = & \mu(x)\partial_x \tilde{\beta}(x,t) + \theta(x)\tilde{\alpha}(x,t) \\ & + \int_0^x h(x,\xi)\tilde{\alpha}(\xi,t)d\xi, \end{aligned} \quad (38)$$

with boundary conditions

$$\tilde{\alpha}(0,t) = 0, \quad \tilde{\beta}(1,t) = 0, \quad (39)$$

where  $g(x,\xi)$  and  $h(x,\xi)$  are functions to be determined. The stability of the target system governed by (37)–(39) and in relation to that of the error dynamics (31)–(34) was demonstrated in Lemma 3.3 [29].

To transform (31)–(34) into (37)–(39), the kernels of (35)

and (36) must adhere to the following PDEs

$$\lambda(x)\partial_x m_1 - \mu(\xi)\partial_\xi m_1 = \mu'(\xi)m_1 + \delta(x)m_1 + \omega(x)m_2, \quad (40)$$

$$\mu(x)\partial_x m_2 + \mu(\xi)\partial_\xi m_2 = -\mu'(\xi)m_2 - \theta(x)m_1, \quad (41)$$

with boundary conditions

$$m_1(x,x) = \frac{\omega(x)}{\lambda(x) + \mu(x)}, \quad (42)$$

$$m_2(1,\xi) = 0. \quad (43)$$

The kernels PDEs, as specified in (40)–(43) is defined over the triangular domain  $\mathcal{T} = \{(x,\xi) \mid 0 \leq \xi \leq x \leq 1\}$ . It is a coupled  $2 \times 2$  *Goursat-form PDEs* governing two kernels equations and the coefficient  $g$  and  $h$  are specified such that

$$g(x,\xi) = -\theta(\xi)m_1(x,\xi) - \int_\xi^x m_1(x,s)h(s,\xi)ds, \quad (44)$$

$$h(x,\xi) = -\theta(\xi)m_2(x,\xi) - \int_\xi^x m_2(x,s)h(s,\xi)ds. \quad (45)$$

The invertibility of the transformation (10) together with the existence of unique solution to (15)–(18) is established in [29]. It consequently implies equivalent stability properties of the target system (37)–(39) and the original system (31)–(34), and

$$p_1(x) = m_1(x,0)\mu(0), \quad (46)$$

$$p_2(x) = m_2(x,0)\mu(0). \quad (47)$$

The inverse transformation of (36) is given by

$$\tilde{\beta}(x,t) = \tilde{v}(x,t) + \int_0^x r_2(x,\xi)\tilde{v}(\xi,t)d\xi, \quad (48)$$

where  $r_2(x,\xi)$  satisfies

$$r_2(x,\xi) = -m_2(x,\xi) - \int_\xi^x m_2(x,s)r_2(s,\xi)ds. \quad (49)$$

The substitution of (48) into (35) results in

$$\begin{aligned} \tilde{\alpha}(x,t) = & \tilde{u}(x,t) - \int_0^x m_1(x,\xi)\left(\tilde{v}(\xi,t) \right. \\ & \left. + \int_0^\xi r_2(\xi,s)\tilde{v}(s,t)ds\right)d\xi \\ = & \tilde{u}(x,t) - \int_0^x m_1(x,\xi)\tilde{v}(\xi,t)d\xi \\ & - \int_0^x \int_\xi^x m_1(x,s)r_2(s,\xi)ds\tilde{v}(\xi,t)d\xi \\ = & \tilde{u}(x,t) + \int_0^x r_1(x,\xi)\tilde{v}(\xi,t)d\xi, \end{aligned} \quad (50)$$

where

$$r_1(x,\xi) = -m_1(x,\xi) - \int_\xi^x m_1(x,s)r_2(s,\xi)ds. \quad (51)$$

The exponential stability of the target system governed by (37)–(39) and to that of the error dynamics (31)–(34) is stated in Lemma 3.3 [29]. The invertibility of the transfor-

mation implies the global exponential convergence of the error system in  $L^2$  sense (31)–(34) and the  $L^2$ -Global Exponential Stability of the plant (1)–(4) combined with the observer (25)–(27) and subject to the control law

$$U(t) = \int_0^1 k_1(1, \xi) \hat{u}(\xi, t) d\xi + \int_0^1 k_2(1, \xi) \hat{v}(\xi, t) d\xi. \quad (52)$$

We refer the reader to [29] for more details about the design of the output feedback law (52), turning our attention to the DeepONet designs for the output feedback law.

**Problem statement.** As shown in Figures 1 and 2, our goal is to design NOs to learn the controller and observer gain functions governed by (15)–(18) and (40)–(43), respectively. The plant function coefficients are the inputs of the nonlinear operators defined by these hyperbolic/Goursat PDEs. We first aim to prove a DeepONet approximation to the kernel PDEs by showing the continuity of the mapping from plant PDE coefficients to kernel PDE solutions. The second part of our design consists of the DeepONet encoding of the output-feedback law. Proof-based machine learning designs are presented in this paper.

### 3 Accuracy of Approximation of Backstepping Kernel Operator with DeepONet

#### 3.1 Boundedness of the gain kernel functions

**Lemma 1** For every  $\lambda, \mu \in C^1([0, 1])$ ,  $\sigma, \omega, \theta \in C^0([0, 1])$ , and  $q \in \mathbb{R}$ , the gain kernels  $k_i(x, \xi), m_i(x, \xi)$ ,  $i = 1, 2$  satisfying the PDE systems (15)–(18) and (40)–(43), respectively, has a unique  $C^1(\mathcal{J})$  solution with the following property

$$|k_i(x, \xi)| \leq N_i e^{M_i}, \quad i = 1, 2, \quad \forall (x, \xi) \in \mathcal{J}, \quad (53)$$

$$|m_i(x, \xi)| \leq N_i e^{M_i}, \quad i = 1, 2, \quad \forall (x, \xi) \in \mathcal{J}, \quad (54)$$

where  $N_i > 0$ ,  $M_i > 0$ ,  $i = 1, 2$  are constants.

**Proof.** The proof of Lemma 1 can be found in [29]. ■

#### 3.2 Approximation of the neural operators

We pursue the characterization of the neural operators to learn the gain kernels function-to-function mapping using finite input-output pairs of collected data. Recall that based on the gain kernels PDEs (15)–(18), a neural approximation of the operator  $(\lambda, \mu, \omega, \sigma, \theta, q) \mapsto (k_1, k_2, m_1, m_2)$  is describe by Figure 1.

Define the operator  $\mathcal{K} : (C^1[0, 1])^2 \times (C^0[0, 1])^3 \times \mathbb{R} \mapsto (C^1(\mathcal{J}))^4$ , where

$$\begin{aligned} & \mathcal{K}(\lambda, \mu, \sigma, \omega, \theta, q)(x, \xi) \\ & := (k_1(x, \xi), k_2(x, \xi), m_1(x, \xi), m_2(x, \xi)), \end{aligned} \quad (55)$$

allowing to introduce the operator  $\mathcal{M} : (C^1[0, 1])^2 \times (C^0[0, 1])^3 \times \mathbb{R} \mapsto (C^1(\mathcal{J}))^2 \times (C^0(\mathcal{J}))^4 \times (C^0[0, 1])^2 \times (C^1(\mathcal{J}))^4$  defined by

$$\begin{aligned} & \mathcal{M}(\lambda, \mu, \sigma, \omega, \theta, q)(x, \xi) \\ & := (k_1, k_2, c, \kappa, K_1, K_2, K_3, K_4, K_5, K_6, K_7, K_8), \end{aligned} \quad (56)$$

where

$$K_1(x) = (\lambda(x) + \mu(x))k_1(x, x) + \theta(x), \quad (57)$$

$$K_2(x) = -\lambda(0)qk_1(x, 0) + \mu(0)k_2(x, 0), \quad (58)$$

$$K_3(x, \xi) = -\mu(x)\partial_x k_1 + \lambda(\xi)\partial_\xi k_1 + \lambda'(\xi)k_1 + \sigma(\xi)k_1$$

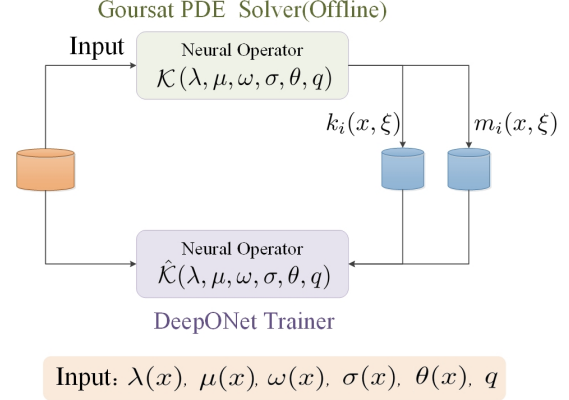


Fig. 1. Learning of the kernel functions via DeepONet and through the operator described by the mapping  $(\lambda, \mu, \omega, \sigma, \theta, q) \rightarrow (k_1, k_2, m_1, m_2)$ . Computing multiple solutions of kernel PDEs (15)–(18) in the Goursat form for different functions  $\lambda(x)$ ,  $\mu(x)$ ,  $\omega(x)$ ,  $\sigma(x)$ ,  $\theta(x)$  and parameters  $q$ , completes the training procedure of the Neural Operator  $\hat{\mathcal{K}}$ .

$$+ \theta(\xi)k_2, \quad (59)$$

$$K_4(x, \xi) = -\mu(x)\partial_x k_2 - \mu(\xi)\partial_\xi k_2 - \mu'(\xi)k_2 + \omega(\xi)k_1, \quad (60)$$

$$K_5(x, \xi) = -\lambda(x)\partial_x m_1 + \mu(\xi)\partial_\xi m_1 - \mu'(\xi)m_1 + \sigma(\xi)m_1 + \omega(x)m_2, \quad (61)$$

$$K_6(x, \xi) = \mu(x)\partial_x m_2 + \mu(\xi)\partial_\xi m_2 + \mu'(\xi)m_2 + \theta(\xi)m_1, \quad (62)$$

$$K_7(x) = m_1(x, x)(\lambda(x) + \mu(x)) - \omega(x), \quad (63)$$

$$K_8(\xi) = m_2(1, \xi), \quad (64)$$

is introduced. The operators  $\mathcal{K}$  and  $\mathcal{M}$  are useful to state the following theorem.

#### Theorem 1 [DeepONet approximation of kernels]

Consider the neural operator defined in (56), along with (57)–(60) and let  $B_\lambda, B_\mu, B_\sigma, B_\omega, B_\theta, B_{\lambda'}, B_{\mu'} > 0$  be arbitrarily large and  $\epsilon > 0$ , there exists a neural operator  $\hat{\mathcal{M}} : (C^1[0, 1])^2 \times (C^0[0, 1])^3 \times \mathbb{R} \mapsto (C^1(\mathcal{J}))^2 \times (C^0(\mathcal{J}))^2 \times (C^0[0, 1])^2 \times (C^1(\mathcal{J}))^4$  such that,

$$|\mathcal{M}(\lambda, \mu, \sigma, \omega, \theta, q)(x, \xi) - \hat{\mathcal{M}}(\lambda, \mu, \sigma, \omega, \theta, q)(x, \xi)| < \epsilon, \quad (65)$$

holds for all Lipschitz  $\lambda, \mu, \sigma, \omega, \theta$  and derivations of  $\lambda, \mu$  with properties that  $\|\lambda\|_\infty \leq B_\lambda, \|\mu\|_\infty \leq B_\mu, \|\sigma\|_\infty \leq B_\sigma, \|\omega\|_\infty \leq B_\omega, \|\theta\|_\infty \leq B_\theta, \|\lambda'\|_\infty \leq B_{\lambda'}, \|\mu'\|_\infty \leq B_{\mu'}$ , namely, there exists a neural operator  $\hat{\mathcal{K}}$  such that

$$\begin{aligned} & |\tilde{k}_1(x, \xi)| + |\tilde{k}_2(x, \xi)| + |\tilde{c}(x, \xi)| + |\tilde{\kappa}(x, \xi)| \\ & + |(\lambda(x) + \mu(x))\tilde{k}_1(x, x)| + |\lambda(0)q\tilde{k}_1(x, 0) - \mu(0)\tilde{k}_2(x, 0)| \\ & + |-\mu(x)\partial_x \tilde{k}_1 + \lambda(\xi)\partial_\xi \tilde{k}_1 + \lambda'(\xi)\tilde{k}_1 + \sigma(\xi)\tilde{k}_1 + \theta(\xi)\tilde{k}_2| \\ & + |-\mu(x)\partial_x \tilde{k}_2 - \mu(\xi)\partial_\xi \tilde{k}_2 - \mu'(\xi)\tilde{k}_2 + \omega(\xi)\tilde{k}_1| \\ & + |\lambda(x)\partial_x \tilde{m}_1 - \mu(\xi)\partial_\xi \tilde{m}_1 + \mu'(\xi)\tilde{m}_1 - \sigma(\xi)\tilde{m}_1 \\ & - \omega(x)\tilde{m}_2 + |\mu(x)\partial_x \tilde{m}_2 + \mu(\xi)\partial_\xi \tilde{m}_2 + \mu'(\xi)\tilde{m}_2 \\ & + \theta(\xi)\tilde{m}_1| < \epsilon, \end{aligned} \quad (66)$$

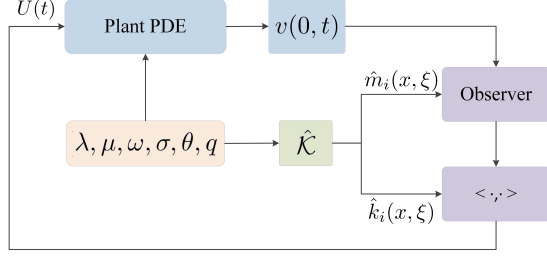


Fig. 2. The PDE backstepping observer (25)–(28) uses boundary measurement of the flux  $v(0, t)$ . The gains  $\hat{k}_i$  and  $\hat{m}_i$ ,  $i = 1, 2$  are produced with the DeepONet  $\hat{\mathcal{K}}$ .

where  $\tilde{c}(x, \xi) = c(x, \xi) - \hat{c}(x, \xi)$ ,  $\tilde{\kappa}(x, \xi) = \kappa(x, \xi) - \hat{\kappa}(x, \xi)$ , and

$$\tilde{k}_i(x, \xi) = k_i(x, \xi) - \hat{k}_i(x, \xi), \quad i = 1, 2, \quad (67)$$

$$\tilde{m}_i(x, \xi) = m_i(x, \xi) - \hat{m}_i(x, \xi), \quad i = 1, 2, \quad (68)$$

and

$$\begin{aligned} &(\hat{k}_1(x, \xi), \hat{k}_2(x, \xi), \hat{m}_1(x, \xi), \hat{m}_2(x, \xi)) \\ &= \hat{\mathcal{K}}(\lambda, \mu, \sigma, \omega, \theta, q)(x, \xi). \end{aligned} \quad (69)$$

**Proof.** The continuity of the operator  $\mathcal{M}$  follows from Lemma 1. The result is obtained by invoking [52, Thm. 2.1]. ■

#### 4 Stabilization under DeepONet Gain Output Feedback

The schematic of the control loop is depicted in Figure 2. We will prove that the gain, a priori learned from the DeepONet layer (offline), enforces closed-loop system stability with a quantifiable exponential decay rate. The system in closed-loop form, consists of the observer (25)–(28) in combination with the output-feedback boundary control law

$$U(t) = \int_0^1 \hat{k}_1(1, \xi) \hat{u}(\xi, t) d\xi + \int_0^1 \hat{k}_2(1, \xi) \hat{v}(\xi, t) d\xi. \quad (70)$$

The backstepping transformations (10), (35) and (36) fed by the approximate gain kernels  $\hat{k}_i(x, \xi)$  and  $\hat{m}_i(x, \xi)$ ,  $i = 1, 2$ , are defined as

$$\hat{u}(x, t) = \hat{u}(x, t), \quad (71)$$

$$\begin{aligned} \hat{z}(x, t) &= \hat{v}(x, t) - \int_0^x \hat{k}_1(x, \xi) \hat{u}(\xi, t) d\xi \\ &\quad - \int_0^x \hat{k}_2(x, \xi) \hat{v}(\xi, t) d\xi, \end{aligned} \quad (72)$$

$$\hat{u}(x, t) = \hat{w}(x, t) + \int_0^x \hat{m}_1(x, \xi) \hat{z}(\xi, t) d\xi, \quad (73)$$

$$\hat{v}(x, t) = \hat{z}(x, t) + \int_0^x \hat{m}_2(x, \xi) \hat{z}(\xi, t) d\xi, \quad (74)$$

where

$$\begin{aligned} &(\hat{k}_1(x, \xi), \hat{k}_2(x, \xi), \hat{m}_1(x, \xi), \hat{m}_2(x, \xi)) \\ &= \hat{\mathcal{K}}(\lambda, \mu, \sigma, \omega, \theta, q)(x, \xi). \end{aligned} \quad (75)$$

Exploiting transformations (72)–(74), the conversion of the observer system (25)–(28) and error system (31)–(34) into a cascaded target system below is achieved

$$\begin{aligned} \partial_t \hat{u}(x, t) &= -\lambda(x) \partial_x \hat{u}(x, t) + \sigma(x) \hat{u}(x, t) + \omega(x) \hat{z}(x, t) \\ &\quad + \int_0^x \hat{c}(x, \xi) \hat{u}(\xi, t) d\xi + \int_0^x \hat{\kappa}(x, \xi) \hat{z}(\xi, t) d\xi \\ &\quad + \hat{m}_1(x, 0) \mu(0) \hat{z}(0, t), \end{aligned} \quad (76)$$

$$\begin{aligned} \partial_t \hat{z}(x, t) &= \mu(x) \partial_x \hat{z}(x, t) + \delta_1(x) \hat{u}(x, t) + \delta_2(x) \hat{z}(0, t) \\ &\quad + \int_0^x \delta_3(x, \xi) \hat{u}(\xi, t) d\xi + \int_0^x \delta_4(x, \xi) \hat{v}(\xi, t) d\xi \\ &\quad + F(x) \mu(0) \hat{z}(0, t), \end{aligned} \quad (77)$$

$$\hat{u}(0, t) = q \hat{z}(0, t), \quad (78)$$

$$\hat{z}(1, t) = 0, \quad (79)$$

$$\begin{aligned} \partial_t \hat{w}(x, t) &= -\lambda(x) \partial_x \hat{w}(x, t) + \sigma(x) \hat{w}(x, t) \\ &\quad + \int_0^x \hat{g}(x, \xi) \hat{w}(\xi, t) d\xi + \int_0^x \delta_5(x, \xi) \hat{z}(\xi, t) d\xi \\ &\quad + \int_0^x \int_\xi^x \hat{r}_1(x, s) \delta_6(s, \xi) ds \hat{z}(\xi, t) d\xi, \end{aligned} \quad (80)$$

$$\begin{aligned} \partial_t \hat{z}(x, t) &= \mu(x) \partial_x \hat{z}(x, t) + \theta(x) \hat{w}(x, t) \\ &\quad + \int_0^x \hat{h}(x, \xi) \hat{w}(\xi, t) d\xi + \int_0^x \delta_6(x, \xi) \hat{z}(\xi, t) d\xi \\ &\quad + \int_0^x \int_\xi^x \hat{r}_2(x, s) \delta_6(s, \xi) ds \hat{z}(\xi, t) d\xi, \end{aligned} \quad (81)$$

$$\hat{w}(0, t) = 0, \quad (82)$$

$$\hat{z}(1, t) = 0, \quad (83)$$

where

$$\begin{aligned} F(x) &= \hat{m}_2(x, 0) - \int_0^x \hat{k}_1(x, \xi) \hat{m}_1(\xi, 0) d\xi \\ &\quad - \int_0^x \hat{k}_2(x, \xi) \hat{m}_2(\xi, 0) d\xi, \end{aligned} \quad (84)$$

$$\hat{g}(x, \xi) = -\theta(\xi) \hat{m}_1(x, \xi) - \theta(\xi) \int_\xi^x \hat{m}_1(x, s) \hat{r}_2(s, \xi) ds, \quad (85)$$

$$\hat{h}(x, \xi) = -\theta(\xi) \hat{m}_2(x, \xi) - \theta(\xi) \int_\xi^x \hat{m}_2(x, s) \hat{r}_2(s, \xi) ds, \quad (86)$$

$$\hat{\kappa}(x, \xi) = \omega(x) \hat{k}_2(x, \xi) + \int_\xi^x \hat{\kappa}(x, s) \hat{k}_2(s, \xi) ds, \quad (87)$$

$$\hat{c}(x, \xi) = \omega(x) \hat{k}_1(x, \xi) + \int_\xi^x \hat{c}(x, s) \hat{k}_1(s, \xi) ds, \quad (88)$$

and  $\delta_i$ ,  $i = 1, 2, \dots, 6$  are defined as

$$\delta_1(x) = (\lambda(x) + \mu(x)) \tilde{k}_1(x, x), \quad (89)$$

$$\delta_2(x) = \lambda(0) q \tilde{k}_1(x, 0) - \mu(0) \tilde{k}_2(x, 0), \quad (90)$$

$$\begin{aligned} \delta_3(x, \xi) &= \lambda(\xi)' \tilde{k}_1(x, \xi) + \sigma(\xi) \tilde{k}_1(x, \xi) + \theta(\xi) \tilde{k}_2(x, \xi) \\ &\quad - \mu(x) \partial_x \tilde{k}_1(x, y) + \lambda(\xi) \partial_\xi \tilde{k}_1(x, \xi), \end{aligned} \quad (91)$$

$$\delta_4(x, \xi) = -\mu(x) \partial_x \tilde{k}_2(x, y) - \mu(\xi) \partial_\xi \tilde{k}_2(x, \xi)$$

$$-\mu(\xi)' \tilde{k}_2(x, \xi) + \omega(\xi) \tilde{k}_1(x, \xi), \quad (92)$$

$$\delta_5(x, \xi) = \lambda(x) \partial_x \tilde{m}_1(x, \xi) - \mu(\xi) \partial_\xi m_1(x, \xi) - \sigma(x) \cdot \tilde{m}_1(x, \xi) - \omega(x) m_2(x, \xi) + \mu(\xi)' \tilde{m}_1(x, \xi), \quad (93)$$

$$\delta_6(s, \xi) = -\mu(s) \partial_s \tilde{m}_2(s, \xi) - \mu(\xi) \partial_\xi \tilde{m}_2(s, \xi) - \mu(\xi)' \tilde{m}_2(s, \xi) - \theta(s) \tilde{m}_1(s, \xi). \quad (94)$$

Note that from (66), the following inequalities hold

$$\|\delta_i\|_\infty \leq \epsilon, \quad i = 1, 2, \dots, 6. \quad (95)$$

We are now poised to state the exponential stability of the target system (76)–(83) in its backstepping-transformed variables; under the DeepONet-approximated kernels.

**Proposition 1 [Lyapunov analysis for DeepONet-perturbed target system]** Consider the cascaded target system (76)–(83), there exists  $\epsilon^* > 0$  such that for all  $\epsilon \in (0, \epsilon^*)$ , the following holds,

$$\Psi_1(t) \leq \Psi_1(0) \vartheta_2 e^{-\vartheta_1(\epsilon)t}, \quad \forall \geq 0, \quad (96)$$

where  $\vartheta_1, \vartheta_2 > 0$  and

$$\Psi_1(t) = \|\hat{u}(t)\|^2 + \|\hat{z}(t)\|^2 + \|\tilde{w}(t)\|^2 + \|\tilde{z}(t)\|^2. \quad (97)$$

**Proof.** As a generalization of the proof in [29], we argue that the following Lyapunov candidate for the target system (76)–(83)

$$V_1(t) = \int_0^1 \frac{\varrho_1 e^{-\varrho_2 x}}{\lambda(x)} \hat{u}(x, t)^2 dx + \int_0^1 \frac{e^{\varrho_2 x}}{\mu(x)} \hat{z}(x, t)^2 dx + \int_0^1 \frac{\varrho_3 e^{-\varrho_4 x}}{\lambda(x)} \tilde{w}(x, t)^2 dx + \int_0^1 \frac{\varrho_5 e^{\varrho_4 x}}{\mu(x)} \tilde{z}(x, t)^2 dx, \quad (98)$$

where  $\varrho_i > 0$ ,  $i = 1, 2, \dots, 5$  are constants to be decided, provides stability at an exponential decay rate to be determined as well.

Computing the time derivative of (98) along (76)–(83) as

$$\begin{aligned} \dot{V}_1(t) = & 2 \int_0^1 \frac{\varrho_1 e^{-\varrho_2 x}}{\lambda(x)} \hat{u}(x, t) \left( -\lambda(x) \partial_x \hat{u}(x, t) \right. \\ & + \sigma(x) \hat{u}(x, t) + \omega(x) \hat{z}(x, t) \\ & + \int_0^x \hat{c}(x, \xi) \hat{u}(\xi, t) d\xi + \int_0^x \hat{\kappa}(x, \xi) \hat{z}(\xi, t) d\xi \\ & + \hat{m}_1(x, 0) \mu(0) \tilde{z}(0, t) \left. \right) + 2 \int_0^1 \frac{e^{\varrho_2 x}}{\mu(x)} \hat{z}(x, t) \\ & \cdot \left( \mu(x) \partial_x \hat{z}(x, t) + \delta_1(x) \hat{u}(x, t) \right. \\ & + \delta_2(x) \hat{z}(0, t) + \int_0^x \delta_3(x, \xi) \hat{u}(\xi, t) d\xi \\ & + \int_0^x \delta_4(x, \xi) \hat{v}(\xi, t) d\xi + F(x) \mu(0) \tilde{z}(0, t) \left. \right) dx \\ & + 2 \int_0^1 \frac{\varrho_3 e^{-\varrho_4 x}}{\lambda(x)} \tilde{w}(x, t) \left( -\lambda(x) \partial_x \tilde{w}(x, t) \right. \\ & + \sigma(x) \tilde{w}(x, t) + \int_0^x \hat{g}(x, \xi) \tilde{w}(\xi, t) d\xi \\ & + \int_0^x \delta_5(x, \xi) \tilde{z}(\xi, t) d\xi \end{aligned}$$

$$\begin{aligned} & + \int_0^x \int_\xi^x \hat{r}_1(x, s) \delta_6(s, \xi) ds \tilde{z}(\xi, t) d\xi \left. \right) \\ & + 2 \int_0^1 \frac{\varrho_5 e^{\varrho_4 x}}{\mu(x)} \tilde{z}(x, t) \left( \mu(x) \partial_x \tilde{z}(x, t) + \theta(x) \tilde{w}(x, t) \right. \\ & + \int_0^x \hat{h}(x, \xi) \tilde{w}(\xi, t) d\xi + \int_0^x \delta_6(x, \xi) \tilde{z}(\xi, t) d\xi \\ & + \int_0^x \int_\xi^x \hat{r}_2(x, s) \delta_6(s, \xi) ds \tilde{z}(\xi, t) d\xi \left. \right) dx, \quad (99) \end{aligned}$$

and using integration by parts and Young's inequality, the following estimate is obtained:

$$\begin{aligned} \dot{V}_1(t) \leq & - \left( \varrho_1 e^{-\varrho_2} \left( \varrho_2 - \frac{2\bar{\sigma} + \bar{\omega} + 2\|\hat{c}\|_\infty + \|\hat{\kappa}\|_\infty}{\lambda} \right. \right. \\ & \left. \left. - \frac{\bar{\mu}\|\hat{m}_1\|_\infty}{\lambda} \right) - \frac{2\epsilon e^{\varrho_2}}{\mu} \right) \|\hat{u}\|^2 \\ & - \left( \varrho_2 - \frac{\varrho_1(\bar{\omega} + \|\hat{\kappa}\|_\infty)}{\lambda} - \frac{\bar{\mu}\bar{F}}{\mu} - \frac{4\epsilon e^{\varrho_2}}{\mu} \right) \|\hat{z}\|^2 \\ & - (1 - \varrho_1 q^2 - \frac{\epsilon e^{\varrho_2}}{\mu}) \hat{z}(0, t)^2 + \frac{\epsilon e^{\varrho_2}}{\mu} \|\hat{v}\|^2 \\ & + \left( \frac{\bar{\mu}\bar{F}}{\mu} e^{2\varrho_2} + \frac{\varrho_1 \bar{\mu} \|\hat{m}_1\|_\infty}{\lambda} \right) \tilde{z}(0, t)^2 \\ & - \left( \varrho_3 \left( \varrho_4 - \frac{2\bar{\sigma}}{\lambda} - \frac{2\bar{\theta}\|\hat{r}_1\|_\infty}{\lambda} \right) e^{-\varrho_4} \right. \\ & \left. - \frac{\varrho_5 \bar{\theta}(1 + \|\hat{r}_2\|_\infty)}{\mu} e^{2\varrho_4} - \frac{\varrho_3 \epsilon(1 + \|\hat{r}_1\|_\infty)}{\lambda} \right) \|\tilde{w}\|^2 \\ & - \left( \varrho_5 \left( \varrho_4 - \frac{\bar{\theta}(1 + \|\hat{r}_2\|_\infty)}{\mu} \right) - \frac{4\epsilon e^{\varrho_4}}{\mu} \right. \\ & \left. - \frac{\varrho_3 \epsilon(1 + \|\hat{r}_1\|_\infty)}{\lambda} \right) \|\tilde{z}\|^2 - \varrho_5 \tilde{z}(0, t)^2, \quad (100) \end{aligned}$$

where  $F(x) \leq \bar{F}$  is a bounded function and

$$\|\hat{c}\|_\infty \leq \bar{\omega} \|\hat{k}_1\|_\infty e^{\|\hat{k}_1\|_\infty}, \quad (101)$$

$$\|\hat{\kappa}\|_\infty \leq \bar{\omega} \|\hat{k}_2\|_\infty e^{\|\hat{k}_2\|_\infty}. \quad (102)$$

Since the inverse transformation of the approximated gain kernel (22) allows to derive a bound of the norm of the state  $v(x, t)$  in (100) with respect to the norm of the approximated target system's state  $\hat{u}(x, t)$  and  $\hat{z}(x, t)$ . In other words,

$$\begin{aligned} \hat{v}(x, t) = & \hat{z}(x, t) + \int_0^x \hat{l}_1(x, \xi) \hat{u}(\xi, t) d\xi \\ & + \int_0^x \hat{l}_2(x, \xi) \hat{z}(\xi, t) d\xi, \quad (103) \end{aligned}$$

where the inverse kernel  $\hat{l}(x, \xi)$  and its inverse  $\hat{k}(x, \xi)$  satisfy the following equation

$$\hat{l}_1(x, \xi) = \hat{k}_1(x, \xi) + \int_\xi^x \hat{k}_2(x, s) \hat{l}_1(s, \xi) ds, \quad (104)$$

$$\hat{l}_2(x, \xi) = \hat{k}_2(x, \xi) + \int_\xi^x \hat{k}_2(x, s) \hat{l}_2(s, \xi) ds, \quad (105)$$

and the following conservative bounds hold

$$\|\hat{l}_1\|_\infty \leq \|\hat{k}_1\|_\infty e^{\|\hat{k}_2\|_\infty}, \quad (106)$$

$$\|\hat{l}_2\|_\infty \leq \|\hat{k}_2\|_\infty e^{\|\hat{k}_2\|_\infty}. \quad (107)$$

Since

$$\|k_i - \hat{k}_i\|_\infty < \epsilon, \quad (108)$$

it follows that

$$\|\hat{k}_i\|_\infty \leq \|k_i\|_\infty + \epsilon, \quad (109)$$

and using (53), we derive the following bound

$$\|\hat{k}_i\|_\infty \leq N_i e^{M_i} + \epsilon. \quad (110)$$

Allowing for the substitution of (110) into (106) and (107) results in the following inequalities

$$\|\hat{l}_1\|_\infty \leq (N_1 e^{M_1} + \epsilon) e^{N_2 e^{M_2} + \epsilon}, \quad (111)$$

$$\|\hat{l}_2\|_\infty \leq (N_2 e^{M_2} + \epsilon) e^{N_2 e^{M_2} + \epsilon}. \quad (112)$$

Similarly, based on the inverse transformations (48) and (50), we have

$$\tilde{w}(x, t) = \tilde{u}(x, t) + \int_0^x \hat{r}_1(x, \xi) \tilde{v}(\xi, t) d\xi, \quad (113)$$

$$\tilde{z}(x, t) = \tilde{v}(x, t) + \int_0^x \hat{r}_2(x, \xi) \tilde{v}(\xi, t) d\xi, \quad (114)$$

where the inverse kernel  $\hat{r}_1(x, \xi)$  and the kernel  $\hat{r}_2(x, \xi)$  satisfy equations

$$\hat{r}_1(x, \xi) = \hat{m}_1(x, \xi) - \int_\xi^x \hat{m}_1(x, s) \hat{r}_2(s, \xi) ds, \quad (115)$$

$$\hat{r}_2(x, \xi) = -\hat{m}_2(x, \xi) - \int_\xi^x \hat{m}_2(x, s) \hat{r}_2(s, \xi) ds, \quad (116)$$

and the following conservative bounds written below hold

$$\|\hat{r}_1\|_\infty \leq \|\hat{m}_1\|_\infty e^{\|\hat{m}_1\|_\infty}, \quad (117)$$

$$\|\hat{r}_2\|_\infty \leq \|\hat{m}_2\|_\infty e^{\|\hat{m}_2\|_\infty}. \quad (118)$$

Knowing that

$$\|m_i - \hat{m}_i\|_\infty < \epsilon, \quad (119)$$

one can deduce that

$$\|\hat{m}_i\|_\infty \leq \|m_i\|_\infty + \epsilon, \quad (120)$$

and using (53) enables one to arrive at

$$\|\hat{m}_i\|_\infty \leq N_i e^{M_i} + \epsilon. \quad (121)$$

Substituting (121) into (117) and (118) gives

$$\|\hat{r}_1\|_\infty \leq (N_1 e^{M_1} + \epsilon) e^{N_1 e^{M_1} + \epsilon}, \quad (122)$$

$$\|\hat{r}_2\|_\infty \leq (N_2 e^{M_2} + \epsilon) e^{N_2 e^{M_2} + \epsilon}. \quad (123)$$

Based on (103), the following relation holds

$$\|v(t)\|^2 = \int_0^1 \left( \hat{z}(x, t) + \int_0^x \hat{l}_1(x, \xi) \hat{u}(\xi, t) d\xi \right)^2 dx$$

$$+ \int_0^x \hat{l}_2(x, \xi) \hat{z}(\xi, t) d\xi \Big)^2 dx \\ \leq 3 \|\hat{l}_1\|_\infty^2 \|\hat{u}(t)\|^2 + 3(1 + \|\hat{l}_2\|_\infty^2) \|\hat{z}(t)\|^2. \quad (124)$$

Substituting (124) into (100) yields the following bound

$$\begin{aligned} \dot{V}_1(t) \leq & - \left( \varrho_1 e^{-\varrho_2} \left( \varrho_2 - \frac{2\bar{\sigma} + \bar{\omega} + 2\|\hat{c}\|_\infty + \|\hat{k}\|_\infty}{\lambda} \right. \right. \\ & \left. \left. - \frac{\bar{\mu}\|\hat{m}_1\|_\infty}{\lambda} \right) - \frac{\epsilon e^{\varrho_2} (2 + 3\|\hat{l}_1\|_\infty^2)}{\mu} \right) \|\hat{u}\|^2 \\ & - \left( \varrho_2 - \frac{\varrho_1(\bar{\omega} + \|\hat{k}\|_\infty)}{\lambda} - \frac{\bar{\mu}\bar{F}}{\mu} - \frac{7\epsilon e^{\varrho_2}}{\mu} \right. \\ & \left. - \frac{3\epsilon e^{\varrho_2} \|\hat{l}_2\|_\infty^2}{\mu} \right) \|\hat{z}\|^2 - (1 - \varrho_1 q^2 - \frac{\epsilon e^{\varrho_2}}{\mu}) \hat{z}(0, t)^2 \\ & - \left( \varrho_3 \left( \varrho_4 - \frac{2\bar{\sigma}}{\lambda} - \frac{2\bar{\theta}\|\hat{r}_1\|_\infty}{\lambda} \right) e^{-\varrho_4} \right. \\ & \left. - \frac{\varrho_5 \bar{\theta} (1 + \|\hat{r}_2\|_\infty)}{\mu} e^{2\varrho_4} - \frac{\varrho_3 \epsilon (1 + \|\hat{r}_1\|_\infty)}{\lambda} \right) \|\tilde{w}\|^2 \\ & - \left( \varrho_5 \left( \varrho_4 - \frac{\bar{\theta} (1 + \|\hat{r}_2\|_\infty)}{\mu} \right) - \frac{4\epsilon e^{\varrho_2}}{\mu} \right. \\ & \left. - \frac{\varrho_3 \epsilon (1 + \|\hat{r}_1\|_\infty)}{\lambda} \right) \|\tilde{z}\|^2 - \left( \varrho_5 - \frac{\bar{\mu}\bar{F}}{\mu} e^{2\varrho_4} \right. \\ & \left. - \frac{\varrho_1 \bar{\mu} \|\hat{m}_1\|_\infty}{\lambda} \right) \tilde{z}(0, t)^2. \quad (125) \end{aligned}$$

Hence, selecting the parameters for the Lyapunov function  $V_1$  as

$$0 < \varrho_1 < \min \left\{ \frac{\lambda(\mu\varrho_2 - \bar{\mu}\bar{F})}{\mu(\bar{\omega} + \|\hat{k}\|_\infty)}, \frac{1}{q^2} \right\}, \quad (126)$$

$$\varrho_2 > \max \left\{ \frac{2\bar{\sigma} + \bar{\omega} + 2\|\hat{c}\|_\infty + \|\hat{k}\|_\infty + \bar{\mu}\|\hat{m}_1\|_\infty}{\lambda}, \frac{\bar{\mu}\bar{F}}{\mu} \right\}, \quad (127)$$

$$\varrho_3 > \frac{\lambda\varrho_5 \bar{\theta} (1 + \|\hat{r}_2\|_\infty) e^{3\varrho_4}}{\mu(\varrho_4 \lambda - 2(\bar{\sigma} + \bar{\theta}\|\hat{r}_1\|_\infty))}, \quad (128)$$

$$\varrho_4 > \max \left\{ \frac{\bar{\theta} (1 + \|\hat{r}_2\|_\infty)}{\mu}, \frac{2\bar{\sigma} + 2\bar{\theta}\|\hat{r}_1\|_\infty}{\lambda} \right\}, \quad (129)$$

$$\varrho_5 > \frac{\bar{\mu}\bar{F} e^{2\varrho_4}}{\mu} + \frac{\varrho_1 \bar{\mu} \|\hat{m}_1\|_\infty}{\lambda}, \quad (130)$$

one can define  $\epsilon^*$  as

$$\begin{aligned} \epsilon^* = \min \left\{ \frac{\mu\varrho_1}{e^{2\varrho_2} (2 + 3\|\hat{l}_1\|_\infty^2)} \left( \varrho_2 - \frac{2\bar{\sigma} + \bar{\omega} + 2\|\hat{c}\|_\infty + \|\hat{k}\|_\infty}{\lambda} \right. \right. \\ \left. \left. - \frac{\bar{\mu}\|\hat{m}_1\|_\infty}{\lambda} \right), \left( \frac{\varrho_2 \lambda - \varrho_1(\bar{\omega} + \|\hat{k}\|_\infty)}{\lambda} - \frac{\bar{\mu}\bar{F}}{\mu} \right) \right. \\ \left. \cdot \frac{\mu}{e^{\varrho_2} (7 + 3\|\hat{l}_2\|_\infty^2)}, \frac{\varrho_5 \lambda (\varrho_4 \mu - \bar{\theta} (1 + \|\hat{r}_2\|_\infty))}{4\lambda e^{\varrho_4} + \mu\varrho_3 (1 + \|\hat{r}_1\|_\infty)} \right. \\ \left. \frac{\lambda}{\varrho_3 (1 + \|\hat{r}_1\|_\infty)} \left( \frac{\varrho_3 (\varrho_4 \lambda - 2(\bar{\sigma} + \bar{\theta}\|\hat{r}_1\|_\infty)) e^{-\varrho_4}}{\lambda} \right) \right\} \end{aligned}$$



$$\left. -\frac{\varrho_5\bar{\theta}(1+\|\hat{r}_2\|_\infty)}{\underline{\mu}}e^{2\varrho_4}\right), \frac{\underline{\mu}(1-\varrho_1q^2)e^{-\varrho_2}}{\underline{\mu}}\left. \right\}, \quad (131)$$

such that for all  $\epsilon \in (0, \epsilon^*)$ ,

$$\dot{V}_1(t) \leq -\vartheta_1 V_1(t), \quad (132)$$

where  $\vartheta_1(\epsilon)$  is defined by

$$\begin{aligned} \vartheta_1(\epsilon) = \min \left\{ \frac{\underline{\lambda}}{\varrho_1} \left( \varrho_1 e^{-\varrho_2} \left( \varrho_2 - \frac{2\bar{\sigma} + \bar{\omega} + 2\|\hat{c}\|_\infty + \|\hat{k}\|_\infty}{\underline{\lambda}} \right. \right. \right. \\ \left. \left. - \frac{\bar{\mu}\|\hat{m}_1\|_\infty}{\underline{\lambda}} \right) - \frac{\epsilon e^{\varrho_2}(2+3\|\hat{l}_1\|_\infty^2)}{\underline{\mu}} \right), \\ \frac{\underline{\mu}}{e^{\varrho_2}} \left( \varrho_2 - \frac{\varrho_1(\bar{\omega} + \|\hat{k}\|_\infty)}{\underline{\lambda}} - \frac{\bar{\mu}\bar{F}}{\underline{\mu}} - \frac{7\epsilon e^{\varrho_2}}{\underline{\mu}} \right. \\ \left. - \frac{3\epsilon e^{\varrho_2}\|\hat{l}_2\|_\infty^2}{\underline{\mu}} \right), \frac{\underline{\lambda}e^{-\varrho_4}}{\varrho_3} \left( \varrho_3 \left( \varrho_4 - \frac{2\bar{\sigma}}{\underline{\lambda}} - \frac{2\bar{\theta}\|\hat{r}_1\|_\infty}{\underline{\lambda}} \right) \right. \\ \left. - \frac{\varrho_5\bar{\theta}(1+\|\hat{r}_2\|_\infty)}{\underline{\mu}} e^{2\varrho_4} - \frac{\varrho_3\epsilon(1+\|\hat{r}_1\|_\infty)}{\underline{\lambda}} \right), \\ \frac{\underline{\mu}}{\varrho_5 e^{\varrho_4}} \left( \varrho_5 \left( \varrho_4 - \frac{\bar{\theta}(1+\|\hat{r}_2\|_\infty)}{\underline{\mu}} \right) - \frac{\varrho_3\epsilon(1+\|\hat{r}_1\|_\infty)}{\underline{\lambda}} \right. \\ \left. - \frac{4\epsilon e^{\varrho_4}}{\underline{\mu}} \right) \left. \right\}, \quad (133) \end{aligned}$$

which leads to the following inequality

$$V_1(t) \leq V_1(0)e^{-\vartheta_1(\epsilon)t}. \quad (134)$$

From (97), we have

$$V_1(t) \leq \max \left\{ \frac{\varrho_1}{\underline{\lambda}}, \frac{\varrho_3}{\underline{\lambda}}, \frac{e^{\varrho_2}}{\underline{\mu}}, \frac{\varrho_5 e^{\varrho_4}}{\underline{\mu}} \right\} \Psi_1(t), \quad (135)$$

$$\Psi_1(t) \leq \frac{1}{\min \left\{ \frac{\varrho_1 e^{-\varrho_2}}{\underline{\lambda}}, \frac{\varrho_3 e^{-\varrho_4}}{\underline{\lambda}}, \frac{1}{\bar{\mu}}, \frac{\varrho_5}{\bar{\mu}} \right\}} V_1(t). \quad (136)$$

Therefore, the exponential stability bound (96) holds, and

$$\begin{aligned} \vartheta_2 = \min \left\{ \frac{\varrho_1 e^{-\varrho_2}}{\underline{\lambda}}, \frac{\varrho_3 e^{-\varrho_4}}{\underline{\lambda}}, \frac{1}{\bar{\mu}}, \frac{\varrho_5}{\bar{\mu}} \right\} \\ \cdot \max \left\{ \frac{\varrho_1}{\underline{\lambda}}, \frac{\varrho_3}{\underline{\lambda}}, \frac{e^{\varrho_2}}{\underline{\mu}}, \frac{\varrho_5 e^{\varrho_4}}{\underline{\mu}} \right\}. \quad (137) \end{aligned}$$

The following proposition is introduced to state the stability equivalence between the target system and the original closed-loop system. There is a norm equivalence between Transformations (72), (74), along with their inverse (103), (113) and (114) help to state the following norm-equivalence properties.

**Proposition 2 [norm equivalence with DeepONet kernels]**  
Consider the closed-loop system including the plant (1)–(4) with observer system (25)–(28) and the observer-based controller (70). There exists  $\epsilon^* > 0$  such that for all  $\epsilon \in (0, \epsilon^*)$ , the following estimates hold between this closed-

loop system and the target system (76)–(83),

$$\Psi_1(t) \leq S_1(\epsilon)\Phi_1(t), \quad \Phi_1(t) \leq S_2(\epsilon)\Psi_1(t), \quad (138)$$

where

$$\Phi_1(t) = \|u(t)\|^2 + \|v(t)\|^2 + \|\hat{u}(t)\|^2 + \|\hat{v}(t)\|^2, \quad (139)$$

$\Psi_1(t)$  is defined in (97) and the positive constants as

$$\begin{aligned} S_1(\epsilon) = 20 + 8(N_1 e^{M_1} + \epsilon) e^{N_1 e^{M_1} + \epsilon} + 8(N_2 e^{M_2} + \epsilon) \\ \cdot e^{N_2 e^{M_2} + \epsilon} + 3(N_1 e^{M_1} + N_2 e^{M_2} + 2\epsilon), \quad (140) \end{aligned}$$

$$\begin{aligned} S_2(\epsilon) = 20 + 9(N_1 e^{M_1} + N_2 e^{M_2} + 2\epsilon) e^{N_2 e^{M_2} + \epsilon} + 4N_1 e^{M_1} \\ + 4N_2 e^{M_2} + 8\epsilon. \quad (141) \end{aligned}$$

**Proof.** From (71)–(74), we have

$$\begin{aligned} \Psi_1(t) = \|\hat{u}(t)\|^2 + \int_0^1 \left( \hat{v}(x, t) - \int_0^x \hat{k}_1(x, \xi) \hat{u}(\xi, t) d\xi \right. \\ \left. - \int_0^x \hat{k}_2(x, \xi) \hat{v}(\xi, t) d\xi \right)^2 dx \\ + \int_0^1 \left( \tilde{u}(x, t) + \int_0^x \hat{r}_1(x, \xi) \tilde{v}(\xi, t) d\xi \right)^2 dx \\ + \int_0^1 \left( \tilde{v}(x, t) + \int_0^x \hat{r}_2(x, \xi) \tilde{v}(\xi, t) d\xi \right)^2 dx \\ \leq \|\hat{u}(t)\|^2 + 3 \int_0^1 \left( \int_0^x \hat{k}_1(x, \xi) \hat{u}(\xi, t) d\xi \right)^2 dx \\ + 3 \|\hat{v}(t)\|^2 + 3 \int_0^1 \left( \int_0^x \hat{k}_2(x, \xi) \hat{v}(\xi, t) d\xi \right)^2 dx \\ + 2 \|\tilde{u}(t)\|^2 + 2 \int_0^1 \left( \int_0^x \hat{r}_1(x, \xi) \tilde{v}(\xi, t) d\xi \right)^2 dx \\ + 2 \|\tilde{v}(t)\|^2 + 2 \int_0^1 \left( \int_0^x \hat{r}_2(x, \xi) \tilde{v}(\xi, t) d\xi \right)^2 dx \\ \leq (1 + 3\|\hat{k}_1\|_\infty^2) \|\hat{u}(t)\|^2 + 3(1 + \|\hat{k}_2\|_\infty^2) \|\hat{v}(t)\|^2 \\ + 2\|\tilde{u}(t)\|^2 + 2(1 + \|\hat{r}_1\|_\infty^2 + \|\hat{r}_2\|_\infty^2) \|\tilde{v}(t)\|^2. \quad (142) \end{aligned}$$

Since  $\tilde{u} = u - \hat{u}$  and  $\tilde{v} = v - \hat{v}$ , we have

$$\begin{aligned} \Psi_1(t) \leq (1 + 3\|\hat{k}_1\|_\infty^2) \|\hat{u}(t)\|^2 + 3(1 + \|\hat{k}_2\|_\infty^2) \|\hat{v}(t)\|^2 \\ + 2\|u(t) - \hat{u}(t)\|^2 + 2(1 + \|\hat{r}_1\|_\infty^2 + \|\hat{r}_2\|_\infty^2) \\ \cdot \|v(t) - \hat{v}(t)\|^2 \\ \leq 4\|u(t)\|^2 + (5 + 3\|\hat{k}_1\|_\infty^2) \|\hat{u}(t)\|^2 + 4(1 + \|\hat{r}_1\|_\infty^2 \\ + \|\hat{r}_2\|_\infty^2) \|v\|^2 + (7 + 4\|\hat{r}_1\|_\infty^2 + 4\|\hat{r}_2\|_\infty^2 + 3\|\hat{k}_2\|_\infty^2) \\ \cdot \|\hat{v}(t)\|^2 \\ \leq (20 + 3\|\hat{k}_1\|_\infty^2 + 3\|\hat{k}_2\|_\infty^2 + 8\|\hat{r}_1\|_\infty^2 + 8\|\hat{r}_2\|_\infty^2) \Phi_1(t). \quad (143) \end{aligned}$$

Submitting (110), (122), and (123) into (143), it arrives

$$\Psi_1(t) \leq \left( 20 + 8(N_1 e^{M_1} + \epsilon) e^{N_1 e^{M_1} + \epsilon} + 8(N_2 e^{M_2} + \epsilon) \right)$$

$$\cdot e^{N_2 e^{M_2 + \epsilon}} + 3(N_1 e^{M_1} + N_2 e^{M_2} + 2\epsilon) \Phi_1(t). \quad (144)$$

Similarly, from (73), (74), and (103), we obtain

$$\begin{aligned} \Phi_1(t) &= \|\hat{u}(t) + \tilde{u}(t)\|^2 + \|\hat{v}(t) + \tilde{v}(t)\|^2 + \|\hat{u}(t)\|^2 + \|\hat{v}(t)\|^2 \\ &\leq 3\|\hat{u}(t)\|^2 + 3 \int_0^1 \left( \hat{z}(x,t) + \int_0^x \hat{l}_1(x,\xi) \hat{u}(\xi,t) d\xi \right. \\ &\quad \left. + \int_0^x \hat{l}_2(x,\xi) \hat{z}(\xi,t) d\xi \right)^2 dx + 2 \int_0^1 \left( \tilde{w}(x,t) \right. \\ &\quad \left. + \int_0^x \hat{m}_1(x,\xi) \hat{z}(\xi,t) d\xi \right)^2 dx + 2 \int_0^1 \left( \hat{z}(x,t) \right. \\ &\quad \left. + \int_0^x \hat{m}_2(x,\xi) \hat{z}(\xi,t) d\xi \right)^2 dx \\ &\leq (3 + 9\|\hat{l}_1\|_\infty^2) \|\hat{u}(t)\|^2 + 9(1 + \|\hat{l}_2\|_\infty^2) \|\hat{z}(t)\|^2 \\ &\quad + 4\|\tilde{w}(t)\|^2 + 4(1 + \|\hat{m}_1\|_\infty^2 + \|\hat{m}_2\|_\infty^2) \|\hat{z}(t)\|^2 \\ &\leq (20 + 9(N_1 e^{M_1} + N_2 e^{M_2} + 2\epsilon)) e^{N_2 e^{M_2 + \epsilon}} \\ &\quad + 4N_1 e^{M_1} + 4N_2 e^{M_2} + 8\epsilon) \Psi_1(t), \end{aligned} \quad (145)$$

which completes the proof.  $\blacksquare$

After establishing the norm-equivalence in Proposition 2, the main result immediately follows in Theorem 2.

### Theorem 2 [main result—stabilization with DeepONet]

Consider the closed-loop system consisting of the plant (1)–(4) together with the observer (25)–(28) and the control law (70). Assuming that functions  $\lambda, \mu \in C^1([0,1])$  have Lipschitz derivatives,  $\sigma, \omega, \theta \in C^0([0,1])$ ,  $q \in \mathbb{R}$ , and satisfy  $\|\lambda\|_\infty \leq B_\lambda$ ,  $\|\mu\|_\infty \leq B_\mu$ ,  $\|\sigma\|_\infty \leq B_\sigma$ ,  $\|\omega\|_\infty \leq B_\omega$ ,  $\|\theta\|_\infty \leq B_\theta$ ,  $\|\lambda'\|_\infty \leq B_{\lambda'}$ ,  $\|\mu'\|_\infty \leq B_{\mu'}$ , where  $B_\lambda, B_\mu, B_\sigma, B_\omega, B_\theta, B_{\lambda'}, B_{\mu'} > 0$  are arbitrarily large constants, there exists a sufficiently small  $\epsilon^*(B_\lambda, B_\mu, B_\sigma, B_\omega, B_\theta, B_{\lambda'}, B_{\mu'}) > 0$  such that all gain in the feedback law (70) and the observer system (25)–(28) with the neural operator  $\hat{\mathcal{M}}(\lambda, \mu, \sigma, \omega, \theta, q)$  of approximation accuracy  $\epsilon \in (0, \epsilon^*)$  in relation to the exact backstepping kernels  $k_i(x, \xi)$ , and  $m_i(x, \xi)$ ,  $i = 1, 2$  that ensures the following exponential stability bound

$$\Phi_1(t) \leq \Phi_1(0) S_1(\epsilon) S_2(\epsilon) \vartheta_2 e^{-\vartheta_1(\epsilon)t}, \quad \forall t \geq 0, \quad (146)$$

where,  $\vartheta_1, \vartheta_2 > 0$  are positive constants,  $\Phi_1(t)$ ,  $S_1(\epsilon)$  and  $S_2(\epsilon)$  are defined in (139)–(141), respectively.

**Remark 1** The product  $S_1 S_2$  is the portion of the overshoot which depends on  $\epsilon$  and this dependence is clearly increasing, based on (140) and (141). It makes sense that poor approximation increases the overshoot estimate. The definition of the decay rate  $\vartheta_1$ , as given (133), shows a decreasing dependence on  $\epsilon$ , meaning that a poor approximation reduces the decay rate estimate.

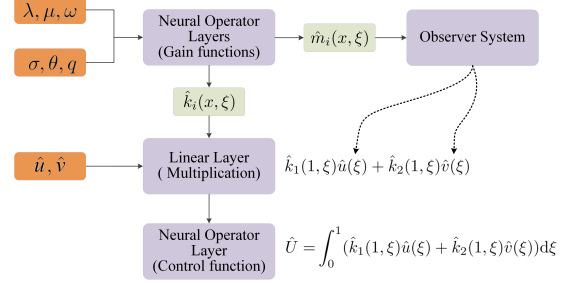


Fig. 3. The learning architecture of the observer-based control law in three steps.

## 5 A Fully Learned Output Feedback Law via DeepONet approximation

### 5.1 Summary of the design procedure

In this section, we present a DeepONet approximation design that enables one to achieve learning of the output-feedback boundary control signal and provide proof-equipped stability guarantees. Exploiting the kernel functions approximation obtained in Section 4, we design a DeepONet that takes as entries the five plant's parameters  $\lambda(x)$ ,  $\mu(x)$ ,  $\sigma(x)$ ,  $\omega(x)$ ,  $\theta(x)$  and  $q$ , as well as the estimates generated by the state observer, namely,  $\hat{u}(x, t)$ ,  $\hat{v}(x, t)$ . The Learning network is built for complete learning of control law restated below for the sake of clarity

$$\hat{U}(t) = \int_0^1 \hat{k}_1(1, \xi) \hat{u}(\xi, t) d\xi + \int_0^1 \hat{k}_2(1, \xi) \hat{v}(\xi, t) d\xi. \quad (147)$$

The structure of the DeepONet-assisted closed-loop system is depicted in Fig. 3. The expansion of the mapping  $\mathcal{K}$  from a larger space  $\mathcal{U}$  to the scalar value of the control input comes at the price of substantial amount of training and learning effort. Furthermore, our result only ensures semi-global practical exponential stability (SG-PES) because as opposed to the approach presented in Section 4, which only contains multiplicative error, the mapping  $\hat{U}(t)$  as reflected in (147), involves an additive intermediate linear layer that supplements additive error into the NO approximation process. We proceed with the three following steps (see Fig. 3):

- **Step 1.** The functions  $\lambda(x)$ ,  $\mu(x)$ ,  $\sigma(x)$ ,  $\omega(x)$ ,  $\theta(x)$ ,  $q$  remain the inputs of through neural operators  $\mathcal{K}$  introduced in Section 4 and generates the NO approximated kernel functions  $\hat{k}_i(x, \xi)$  and  $\hat{m}_i(x, \xi)$ ,  $i = 1, 2$ .
- **Step 2.** A linear layer is utilized to multiply the estimated kernel functions  $\hat{k}_i(x, \xi)$ ,  $i = 1, 2$  with the observer's estimates  $\hat{u}$  and  $\hat{v}$ .
- **Step 3.** A new neural operator  $\mathcal{U} : (\lambda, \mu, \sigma, \omega, \theta, q, \hat{u}, \hat{v}) \mapsto U$ ,  $(C^1[0,1])^2 \times (C^0[0,1])^3 \times \mathbb{R} \times (C^0[0,1])^2 \mapsto \mathbb{R}$ , where  $U$  is defined in (70), is learned to implement the nonlinear integral operation, resulting in the final observer-based control law  $\hat{U}$  given by (147). This mapping is developed using the DeepONet approximation accuracy theorem recently introduced in [41] for a reaction-diffusion PDE.

The expansion of the mapping  $\mathcal{K}$  defined in **Step 1** from

larger space  $\mathcal{U}$  to the scalar value of the control input  $\hat{U}(t)$  comes at the price of a substantial amount of training and learning effort.

Let's denote  $\hat{\mathcal{U}}$  the NO approximation of the output-feedback operator  $\mathcal{U} : (\lambda, \mu, \sigma, \omega, \theta, q, \hat{u}, \hat{v}) \mapsto U, (C^1[0, 1])^2 \times (C^0[0, 1])^3 \times \mathbb{R} \times (C^0[0, 1])^2 \mapsto \mathbb{R}$ , and recall the operator  $\hat{\mathcal{M}}$  given in Theorem 1, the following theorem holds.

**Theorem 3** *Let  $B_\lambda, B_\mu, B_\sigma, B_\omega, B_\theta, B_{\lambda'}, B_{\mu'} > 0$  be arbitrarily large and  $\epsilon > 0$ , there exists neural operators  $\hat{\mathcal{M}}$  and  $\hat{\mathcal{U}}$  such that*

$$\begin{aligned} & |\mathcal{U}(\lambda, \mu, \sigma, \omega, \theta, q, \hat{u}, \hat{v}) - \hat{\mathcal{U}}(\lambda, \mu, \sigma, \omega, \theta, q, \hat{u}, \hat{v})| \\ & + |\mathcal{M}(\lambda, \mu, \sigma, \omega, \theta, q)(x, \xi) - \hat{\mathcal{M}}(\lambda, \mu, \sigma, \omega, \theta, q)(x, \xi)| < \epsilon, \end{aligned} \quad (148)$$

holds for all Lipschitz  $\lambda, \mu, \sigma, \omega, \theta, \hat{u}, \hat{v}$  with the properties that  $\|\lambda\|_\infty \leq B_\lambda, \|\mu\|_\infty \leq B_\mu, \|\sigma\|_\infty \leq B_\sigma, \|\omega\|_\infty \leq B_\omega, \|\theta\|_\infty \leq B_\theta, \|\lambda'\|_\infty \leq B_{\lambda'}, \|\mu'\|_\infty \leq B_{\mu'}, \|\hat{u}(t)\|_\infty \leq B_u, \|\hat{v}(t)\|_\infty \leq B_v$ , namely, there exists neural operators  $\hat{\mathcal{X}}$  such that

$$\begin{aligned} & |\tilde{k}_1| + |\tilde{k}_2| + |\tilde{c}| + |\tilde{k}| + |(\lambda(x) + \mu(x))\tilde{k}_1(x, x)| \\ & + |\lambda(0)q\tilde{k}_1(x, 0) - \mu(0)\tilde{k}_2(x, 0)| \\ & + |-\mu(x)\partial_x\tilde{k}_1 + \lambda(\xi)\partial_\xi\tilde{k}_1 + \lambda'(\xi)\tilde{k}_1 + \sigma(\xi)\tilde{k}_1 + \theta(\xi)\tilde{k}_2| \\ & + |-\mu(x)\partial_x\tilde{k}_2 - \mu(\xi)\partial_\xi\tilde{k}_2 - \mu'(\xi)\tilde{k}_2 + \omega(\xi)\tilde{k}_1| \\ & + |\lambda(x)\partial_x\tilde{m}_1 - \mu(\xi)\partial_\xi\tilde{m}_1 + \mu'(\xi)\tilde{m}_1 - \sigma(\xi)\tilde{m}_1 - \omega(x)\tilde{m}_2| \\ & + |\mu(x)\partial_x\tilde{m}_2 + \mu(\xi)\partial_\xi\tilde{m}_2 + \mu'(\xi)\tilde{m}_2 + \theta(\xi)\tilde{m}_1| \\ & + |\hat{\mathcal{U}}(\lambda, \mu, \sigma, \omega, \theta, q, \hat{u}, \hat{v})| < \epsilon. \end{aligned} \quad (149)$$

**Proof.** The continuity of the operator  $\mathcal{M}$  follows directly from Lemma 1 and that of the operator  $\mathcal{U}$  can be established following [40, Lem. 4]. The final result is then obtained by invoking [52, Thm. 2.1].  $\blacksquare$

Theorem 3 is used to prove the stability of (1)–(4) combined with the observer system (25)–(28) when the approximated output feedback control law (147) learned through DeepOnet is assigned. By collecting training input-output data generated by a range of constants  $q$  and a family of spatially varying parameter functions  $\lambda(x), \mu(x), \sigma(x), \omega(x), \theta(x)$  as well as the observer states  $\hat{u}(x)$  and  $\hat{v}(x)$ .

## 5.2 Stabilization under output feedback control law generated via DeepOnet

Recalling the NO approximation  $\hat{\mathcal{U}}$ , the approximated control (147) can be expressed as  $\hat{U} = \hat{\mathcal{U}}(\lambda, \mu, \sigma, \omega, \theta, q, \hat{u}, \hat{v})$ . Applying the certainty equivalence principle, the approximated backstepping transformations (10), (35) and (36) fed by the  $\tilde{k}_i$  and  $\tilde{m}_i, i = 1, 2$ , are defined as (72)–(74), respectively. The inverse transformations of (72)–(74) are defined in (103), (113) and (114), respectively.

Using the backstepping transformation (72), the observer (28)–(25) translates into the following target system

$$\partial_t \hat{u}(x, t) = -\lambda(x)\partial_x \hat{u}(x, t) + \sigma(x)\hat{u}(x, t) + \omega(x)\hat{z}(x, t)$$

$$\begin{aligned} & + \int_0^x c(x, \xi)\hat{u}(\xi, t)d\xi + \int_0^x \kappa(x, \xi)\hat{z}(\xi, t)d\xi \\ & + \hat{m}_1(x, 0)\mu(0)\tilde{z}(0, t), \end{aligned} \quad (150)$$

$$\partial_t \hat{z}(x, t) = \mu(x)\partial_x \hat{z}(x, t) + F(x)\mu(0)\tilde{z}(0, t), \quad (151)$$

$$\hat{u}(0, t) = q\tilde{z}(0, t), \quad (152)$$

$$\hat{z}(1, t) = \tilde{U}(t), \quad (153)$$

where  $\hat{\kappa}(x, \xi), \hat{c}(x, \xi)$  and  $F(x)$  are defined in (87), (88), and (84), respectively. The approximation error terms,  $\delta_i, i = 1, 2, 3, 4$  are given in (89)–(92), and  $\tilde{U}(t) = U(t) - \hat{U}(t)$ . We recall that  $U(t)$ , the approximated control law (147), is obtained from an approximation of the gain kernel when functions parameters  $\lambda(x), \mu(x), \sigma(x), \omega(x), \theta(x)$  vary whereas the full approximation of the feedback law, namely,  $\hat{U}(t)$ , requires input-output data of the observer states, namely,  $\hat{u}$  and  $\hat{v}$ , provided some  $L^2$  initial data  $(u_0(x), v_0(x), \hat{u}_0(x), \hat{v}_0(x))$ . It is worth recalling that the estimated state trajectories are derived from a dataset collected at the sensing point  $v(0, t)$ .

Using (73)–(74), the error system (31)–(34) maps into the following set of PDEs

$$\begin{aligned} \partial_t \tilde{w}(x, t) & = -\lambda(x)\partial_x \tilde{w}(x, t) + \sigma(x)\tilde{w}(x, t) \\ & + \int_0^x \hat{g}(x, \xi)\tilde{w}(\xi, t)d\xi + \int_0^x \delta_5(x, \xi)\tilde{z}(\xi, t)d\xi \\ & + \int_0^x \int_\xi^x \hat{r}_1(x, s)\delta_6(s, \xi)ds\tilde{z}(\xi, t)d\xi, \end{aligned} \quad (154)$$

$$\begin{aligned} \partial_t \tilde{z}(x, t) & = \mu(x)\partial_x \tilde{z}(x, t) + \theta(x)\tilde{w}(x, t) \\ & + \int_0^x \hat{h}(x, \xi)\tilde{w}(\xi, t)d\xi + \int_0^x \delta_6(x, \xi)\tilde{z}(\xi, t)d\xi \\ & + \int_0^x \int_\xi^x \hat{r}_2(x, s)\delta_6(s, \xi)ds\tilde{z}(\xi, t)d\xi, \end{aligned} \quad (155)$$

$$\tilde{w}(0, t) = 0, \quad (156)$$

$$\tilde{z}(1, t) = \tilde{U}(t). \quad (157)$$

where  $\hat{g}(x, \xi), \hat{h}(x, \xi), \delta_5(x, \xi)$  and  $\delta_6(x, \xi)$  are defined in (85), (86), (93) and (94), respectively.

Our first result for the coupled target system (150)–(153), (154)–(157) is its semi-global practical exponential stability in the backstepping-transformed variables under the DeepOnet-approximated kernels.

**Proposition 3** *Consider the cascaded target system (150)–(153), (154)–(157), there exists  $\epsilon^* > 0$  such that for all  $\epsilon \in (0, \epsilon^*)$ , and the following holds,*

$$\Psi_2(t) \leq \Psi_2(0)\vartheta_4 e^{-\vartheta_3(\epsilon)t} + \vartheta_5 \epsilon^2, \quad \forall t \geq 0, \quad (158)$$

where  $\vartheta_i > 0, i = 3, 4, 5$ , and

$$\Psi_2(t) = \|\hat{u}(t)\|^2 + \|\hat{z}(t)\|^2 + \|\tilde{w}(t)\|^2 + \|\tilde{z}(t)\|^2. \quad (159)$$

**Proof.** Define the Lyapunov function

$$V_2(t) = \int_0^1 \frac{\iota_1 e^{-\iota_2 x}}{\lambda(x)} \hat{u}(x, t)^2 dx + \int_0^1 \frac{e^{\iota_2 x}}{\mu(x)} \hat{z}(x, t)^2 dx$$

$$+ \int_0^1 \frac{\iota_3 e^{-\iota_4 x}}{\lambda(x)} \tilde{w}(x, t)^2 dx + \int_0^1 \frac{\iota_5 e^{\iota_4 x}}{\mu(x)} \tilde{z}(x, t)^2 dx, \quad (160)$$

where  $\iota_i > 0$ ,  $i = 1, 2, \dots, 5$  are constants to be selected.

Computing the time derivative of (160) along (150)–(153), (154)–(157) as

$$\begin{aligned} \dot{V}_2(t) = & 2 \int_0^1 \frac{\iota_1 e^{-\iota_2 x}}{\lambda(x)} \hat{u}(x, t) \left( -\lambda(x) \partial_x \hat{u}(x, t) \right. \\ & + \sigma(x) \hat{u}(x, t) + \omega(x) \hat{z}(x, t) \\ & + \int_0^x c(x, \xi) \hat{u}(\xi, t) d\xi + \int_0^x \kappa(x, \xi) \hat{z}(\xi, t) d\xi \\ & \left. + \hat{m}_1(x, 0) \mu(0) \tilde{z}(0, t) \right) + 2 \int_0^1 \frac{e^{\iota_2 x}}{\mu(x)} \hat{z}(x, t) \\ & \cdot \left( \mu(x) \partial_x \hat{z}(x, t) + F(x) \mu(0) \tilde{z}(0, t) \right) dx \\ & + 2 \int_0^1 \frac{\iota_3 e^{-\iota_4 x}}{\lambda(x)} \tilde{w}(x, t) \left( -\lambda(x) \partial_x \tilde{w}(x, t) \right. \\ & + \sigma(x) \tilde{w}(x, t) + \int_0^x \hat{g}(x, \xi) \tilde{w}(\xi, t) d\xi \\ & + \int_0^x \delta_5(x, \xi) \tilde{z}(\xi, t) d\xi \\ & \left. + \int_0^x \int_\xi^x \hat{r}_1(x, s) \delta_6(s, \xi) ds \tilde{z}(\xi, t) d\xi \right) dx \\ & + 2 \int_0^1 \frac{\iota_5 e^{\iota_4 x}}{\mu(x)} \tilde{z}(x, t) \left( \mu(x) \partial_x \tilde{z}(x, t) + \theta(x) \tilde{w}(x, t) \right. \\ & + \int_0^x \hat{h}(x, \xi) \tilde{w}(\xi, t) d\xi + \int_0^x \delta_6(x, \xi) \tilde{z}(\xi, t) d\xi \\ & \left. + \int_0^x \int_\xi^x \hat{r}_2(x, s) \delta_6(s, \xi) ds \tilde{z}(\xi, t) d\xi \right) dx, \quad (161) \end{aligned}$$

and using integration by parts and Young's inequality, the following estimate is derived

$$\begin{aligned} \dot{V}_2(t) \leq & -\iota_1 e^{-\iota_2} \left( \iota_2 - \frac{2\bar{\sigma} + \bar{\omega} + 2\|c\|_\infty + \|\kappa\|_\infty}{\lambda} \right. \\ & - \frac{\bar{\mu} \|\hat{m}_1\|_\infty}{\lambda} \left. \right) \|\hat{u}\|^2 - \left( \iota_2 - \frac{\iota_1(\bar{\omega} + \|\kappa\|_\infty)}{\lambda} \right. \\ & - \frac{\bar{\mu} \bar{F}}{\mu} \left. \right) \|\hat{z}\|^2 - (1 - \iota_1 q^2) \hat{z}(0, t)^2 + e^{\iota_2} \hat{z}(1, t)^2 \\ & + \left( \frac{\bar{\mu} \bar{F}}{\mu} e^{2\iota_2} + \frac{\iota_1 \bar{\mu} \|\hat{m}_1\|_\infty}{\lambda} \right) \tilde{z}(0, t)^2 \\ & - \left( \iota_3 \left( \iota_4 - \frac{2\bar{\sigma}}{\lambda} - \frac{2\bar{\theta} \|\hat{r}_1\|_\infty}{\lambda} \right) e^{-\iota_4} \right. \\ & - \frac{\iota_5 \bar{\theta} (1 + \|\hat{r}_2\|_\infty)}{\mu} e^{2\iota_4} - \frac{\iota_1 \epsilon (1 + \|\hat{r}_1\|_\infty)}{\lambda} \left. \right) \|\tilde{w}\|^2 \\ & - \iota_5 \tilde{z}(0, t)^2 - \left( \iota_5 \left( \iota_4 - \frac{\bar{\theta} (1 + \|\hat{r}_2\|_\infty)}{\mu} \right) - \frac{4\epsilon e^{\iota_4}}{\mu} \right. \\ & \left. - \frac{\iota_3 \epsilon (1 + \|\hat{r}_1\|_\infty)}{\lambda} \right) \|\tilde{z}\|^2 + \iota_5 e^{\iota_4} \tilde{z}(1, t)^2, \quad (162) \end{aligned}$$

where

$$\|c\|_\infty \leq \bar{\omega} \|k_1\|_\infty e^{\|k_1\|_\infty}, \quad (163)$$

$$\|\kappa\|_\infty \leq \bar{\omega} \|k_2\|_\infty e^{\|k_2\|_\infty}. \quad (164)$$

Substituting (53) into (163) and (164), we get

$$\|c\|_\infty \leq \bar{\omega} N_1 e^{M_1 + N_1 e^{M_1}}, \quad (165)$$

$$\|\kappa\|_\infty \leq \bar{\omega} N_2 e^{M_2 + N_2 e^{M_2}}. \quad (166)$$

Since we have designed the neural operator  $\mathcal{U}$  to learn the mapping  $(\lambda, \mu, \delta, \omega, \theta, u, v) \mapsto U$  such that  $\hat{U}(t) = \mathcal{U}(\lambda, \mu, \delta, \omega, \theta, q, \hat{u}(t), \hat{v}(t))$ , we can get  $|U(t) - \hat{U}(t)| \leq \epsilon$ . Hence, the estimate below can be derived

$$\begin{aligned} \dot{V}_2(t) = & -\iota_1 e^{-\iota_2} \left( \iota_2 - \frac{2\bar{\sigma} + \bar{\omega} + 2\|c\|_\infty + \|\kappa\|_\infty}{\lambda} \right. \\ & - \frac{\bar{\mu} \|\hat{m}_1\|_\infty}{\lambda} \left. \right) \|\hat{u}\|^2 - \left( \iota_2 - \frac{\iota_1(\bar{\omega} + \|\kappa\|_\infty)}{\lambda} \right. \\ & - \frac{\bar{\mu} \bar{F}}{\mu} \left. \right) \|\hat{z}\|^2 - (1 - \iota_1 q^2) \hat{z}(0, t)^2 \\ & - \left( \iota_5 - \frac{\bar{\mu} \bar{F}}{\mu} e^{2\iota_2} - \frac{\iota_1 \bar{\mu} \|\hat{m}_1\|_\infty}{\lambda} \right) \tilde{z}(0, t)^2 \\ & - \left( \iota_3 \left( \iota_4 - \frac{2\bar{\sigma}}{\lambda} - \frac{2\bar{\theta} \|\hat{r}_1\|_\infty}{\lambda} \right) e^{-\iota_4} \right. \\ & - \frac{\iota_5 \bar{\theta} (1 + \|\hat{r}_2\|_\infty)}{\mu} e^{2\iota_4} - \frac{\iota_1 \epsilon (1 + \|\hat{r}_1\|_\infty)}{\lambda} \left. \right) \|\tilde{w}\|^2 \\ & - \left( \iota_5 \left( \iota_4 - \frac{\bar{\theta} (1 + \|\hat{r}_2\|_\infty)}{\mu} \right) - \frac{4\epsilon e^{\iota_4}}{\mu} \right. \\ & \left. - \frac{\iota_3 \epsilon (1 + \|\hat{r}_1\|_\infty)}{\lambda} \right) \|\tilde{z}\|^2 + (e^{\iota_2} + \iota_5 e^{\iota_4}) \epsilon^2. \quad (167) \end{aligned}$$

For the time-derivative of the Lyapunov function  $V_2(t)$ . We can set that

$$0 < \iota_1 < \frac{1}{q^2}, \quad (168)$$

$$\iota_2 > \max \left\{ \frac{2\bar{\sigma} + \bar{\omega} + 2\|c\|_\infty + \|\kappa\|_\infty + \bar{\mu} \|\hat{m}_1\|_\infty}{\lambda}, \frac{\iota_1(\bar{\omega} + \|\kappa\|_\infty) + \bar{\mu} \bar{F}}{\lambda} \right\}, \quad (169)$$

$$\iota_3 > \frac{\lambda \iota_5 \bar{\theta} (1 + \|\hat{r}_2\|_\infty) e^{3\iota_4}}{\mu (\iota_4 \lambda - 2(\bar{\sigma} + \bar{\theta} \|\hat{r}_1\|_\infty))}, \quad (170)$$

$$\iota_4 > \max \left\{ \frac{\bar{\theta} (1 + \|\hat{r}_2\|_\infty)}{\mu}, \frac{2\bar{\sigma} + 2\bar{\theta} \|\hat{r}_1\|_\infty}{\lambda} \right\}, \quad (171)$$

$$\iota_5 > \frac{\bar{\mu} \bar{F} e^{2\iota_2}}{\mu} + \frac{\iota_1 \bar{\mu} \|\hat{m}_1\|_\infty}{\lambda}, \quad (172)$$

one can define  $\epsilon^*$  as

$$\epsilon^* = \min \left\{ \frac{\lambda}{\iota_1 (1 + \|\hat{r}_1\|_\infty)} \left( \frac{\iota_3 (\iota_4 \lambda - 2(\bar{\sigma} + \bar{\theta} \|\hat{r}_1\|_\infty)) e^{-\iota_4}}{\lambda} \right. \right.$$

$$\left. - \frac{\iota_5 \bar{\theta}(1 + \|\hat{r}_2\|_\infty)}{\underline{\mu}} e^{2\iota_4} \right), \frac{\iota_5 \lambda (\iota_4 \underline{\mu} - \bar{\theta}(1 + \|\hat{r}_2\|_\infty))}{4\lambda e^{\iota_2} + \underline{\mu} \iota_3 (1 + \|\hat{r}_1\|_\infty)} \left. \right\}, \quad (173)$$

such that for all  $\epsilon \in (0, \epsilon^*)$ ,

$$\dot{V}_2(t) \leq -\vartheta_3(\epsilon) V_2(t) + (e^{\iota_2} + \iota_5 e^{\iota_4}) \epsilon^2, \quad (174)$$

where  $\vartheta_3(\epsilon)$  is defined by

$$\vartheta_3(\epsilon) = \min \left\{ \lambda e^{-\iota_2} \left( \iota_2 - \frac{2\bar{\sigma} + \bar{\omega} + 2\|c\|_\infty + \|\kappa\|_\infty}{\lambda} - \frac{\bar{\mu}\|\hat{m}_1\|_\infty}{\lambda} \right), \frac{\underline{\mu}}{e^{\iota_2}} \left( \iota_2 - \frac{\iota_1(\bar{\omega} + \|\kappa\|_\infty)}{\lambda} - \frac{\bar{\mu}\bar{F}}{\underline{\mu}} \right), \frac{\lambda e^{-\iota_4}}{\iota_3} \left( \iota_3 \left( \iota_4 - \frac{2\bar{\sigma}}{\lambda} - \frac{2\bar{\theta}\|\hat{r}_1\|_\infty}{\lambda} \right) - \frac{\iota_3 \epsilon (1 + \|\hat{r}_1\|_\infty)}{\lambda} - \frac{\iota_5 \bar{\theta}(1 + \|\hat{r}_2\|_\infty)}{\underline{\mu}} e^{2\iota_4} \right), \frac{\underline{\mu}}{\iota_5 e^{\iota_4}} \left( \iota_5 \left( \iota_4 - \frac{\bar{\theta}(1 + \|\hat{r}_2\|_\infty)}{\underline{\mu}} - \frac{4\epsilon e^{\iota_4}}{\underline{\mu}} - \frac{\iota_3 \epsilon (1 + \|\hat{r}_1\|_\infty)}{\lambda} \right) \right) \right\}. \quad (175)$$

Thus, we have the following inequality

$$V_2(t) \leq V_2(0) e^{-\vartheta_3(\epsilon)t} + \frac{e^{\iota_2} + \iota_5 e^{\iota_4}}{\vartheta_3} \epsilon^2. \quad (176)$$

From (159), we have

$$V_2(t) \leq \max \left\{ \frac{\iota_1}{\lambda}, \frac{\iota_3}{\lambda}, \frac{e^{\iota_2}}{\underline{\mu}}, \frac{\iota_5 e^{\iota_4}}{\underline{\mu}} \right\} \Psi_2(t), \quad (177)$$

$$\Psi_2(t) \leq \frac{1}{\min \left\{ \frac{\iota_1 e^{-\iota_2}}{\lambda}, \frac{\iota_3 e^{-\iota_4}}{\lambda}, \frac{1}{\bar{\mu}}, \frac{\iota_5}{\bar{\mu}} \right\}} V_2(t). \quad (178)$$

Therefore, the exponential stability bound (158) holds, and

$$\vartheta_4(\epsilon) = \frac{e^{\iota_2} + \iota_5 e^{\iota_4}}{\vartheta_3(\epsilon)}, \quad (179)$$

$$\vartheta_5 = \min \left\{ \frac{\iota_1 e^{-\iota_2}}{\lambda}, \frac{\iota_3 e^{-\iota_4}}{\lambda}, \frac{1}{\bar{\mu}}, \frac{\iota_5}{\bar{\mu}} \right\} \cdot \max \left\{ \frac{\iota_1}{\lambda}, \frac{\iota_3}{\lambda}, \frac{e^{\iota_2}}{\underline{\mu}}, \frac{\iota_5 e^{\iota_4}}{\underline{\mu}} \right\}, \quad (180)$$

we have completed this proof.  $\blacksquare$

To translate the stability of the cascaded target system into that of the original closed-loop system, we consider transformations (72)–(74), along with inverse transformations (103), (113) and (114), and provide the following proposition.

**Proposition 4 [norm equivalence with DeepONet kernels]**

Consider the closed-loop system including the plant (1)–(4) with observer system (25)–(28) and the observer-based controller (147). There exists  $\epsilon^* > 0$  such that for all  $\epsilon \in (0, \epsilon^*)$ , the following estimates hold between this closed-loop system and the cascaded target system (150)–(153), (154)–(157),

$$\Psi_2(t) \leq S_1(\epsilon) \Phi_2(t), \quad \Phi_2(t) \leq S_2(\epsilon) \Psi_2(t), \quad (181)$$

where

$$\Phi_2(t) = \|u(t)\|^2 + \|v(t)\|^2 + \|\hat{u}(t)\|^2 + \|\hat{v}(t)\|^2, \quad (182)$$

and the positive constants are defined in (140) and (141), respectively.

**Proof.** The proof of Proposition 4 is similar to that of Proposition 2. From (72)–(74), we have

$$\begin{aligned} \Psi_2(t) &= \|\hat{u}(t)\|^2 + \int_0^1 \left( \hat{v}(x, t) - \int_0^x \hat{k}_1(x, \xi) \hat{u}(\xi, t) d\xi - \int_0^x \hat{k}_2(x, \xi) \hat{v}(\xi, t) d\xi \right)^2 dx \\ &\quad + \int_0^1 \left( \tilde{u}(x, t) + \int_0^x \hat{r}_1(x, \xi) \tilde{v}(\xi, t) d\xi \right)^2 dx \\ &\quad + \int_0^1 \left( \tilde{v}(x, t) + \int_0^x \hat{r}_2(x, \xi) \tilde{v}(\xi, t) d\xi \right)^2 dx \\ &\leq \|\hat{u}(t)\|^2 + 3 \int_0^1 \left( \int_0^x \hat{k}_1(x, \xi) \hat{u}(\xi, t) d\xi \right)^2 dx \\ &\quad + 3 \|\hat{v}(t)\|^2 + 3 \int_0^1 \left( \int_0^x \hat{k}_2(x, \xi) \hat{v}(\xi, t) d\xi \right)^2 dx \\ &\quad + 2 \|\tilde{u}(t)\|^2 + 2 \int_0^1 \left( \int_0^x \hat{r}_1(x, \xi) \tilde{v}(\xi, t) d\xi \right)^2 dx \\ &\quad + 2 \|\tilde{v}(t)\|^2 + 2 \int_0^1 \left( \int_0^x \hat{r}_2(x, \xi) \tilde{v}(\xi, t) d\xi \right)^2 dx \\ &\leq (1 + 3 \|\hat{k}_1\|_\infty^2) \|\hat{u}(t)\|^2 + 3(1 + \|\hat{k}_2\|_\infty^2) \|\hat{v}(t)\|^2 \\ &\quad + 2 \|u(t) - \hat{u}(t)\|^2 + 2(1 + \|\hat{r}_1\|_\infty^2 + \|\hat{r}_2\|_\infty^2) \\ &\quad \cdot \|v(t) - \hat{v}(t)\|^2 \\ &\leq (20 + 3 \|\hat{k}_1\|_\infty^2 + 3 \|\hat{k}_2\|_\infty^2 + 8 \|\hat{r}_1\|_\infty^2 + 8 \|\hat{r}_2\|_\infty^2) \Phi_2(t). \end{aligned} \quad (183)$$

Submitting (53), (122), and (123) into (183), it arrives

$$\begin{aligned} \Psi_2(t) &\leq (20 + 8(N_1 e^{M_1} + \epsilon) e^{N_1 e^{M_1} + \epsilon} + 8(N_2 e^{M_2} + \epsilon) \\ &\quad \cdot e^{N_2 e^{M_2} + \epsilon} + 3(N_1 e^{M_1} + N_2 e^{M_2} + 2\epsilon)) \Phi_2(t). \end{aligned} \quad (184)$$

Similarly, from (103), (113) and (114), we obtain

$$\begin{aligned} \Phi_2(t) &\leq 3 \|\hat{u}(t)\|^2 + 3 \|\hat{v}(t)\|^2 + 2 \|\tilde{u}(t)\|^2 + 2 \|\tilde{v}(t)\|^2 \\ &\leq 3 \|\hat{u}(t)\|^2 + 3 \int_0^1 \left( \hat{z}(x, t) + \int_0^x \hat{l}_1(x, \xi) \hat{u}(\xi, t) d\xi \right. \\ &\quad \left. + \int_0^x \hat{l}_2(x, \xi) \hat{z}(\xi, t) d\xi \right)^2 dx + 2 \int_0^1 \left( \tilde{w}(x, t) \right. \\ &\quad \left. + \int_0^x \hat{m}_1(x, \xi) \tilde{z}(\xi, t) d\xi \right)^2 dx + 2 \int_0^1 \left( \tilde{z}(x, t) \right. \\ &\quad \left. + \int_0^x \hat{m}_2(x, \xi) \tilde{z}(\xi, t) d\xi \right)^2 dx \\ &\leq (3 + 9 \|\hat{l}_1\|_\infty^2) \|\hat{u}(t)\|^2 + 9(1 + \|\hat{l}_2\|_\infty^2) \|\hat{z}(t)\|^2 \\ &\quad + 4 \|\tilde{w}(t)\|^2 + 4(1 + \|\hat{m}_1\|_\infty^2 + \|\hat{m}_2\|_\infty^2) \|\tilde{z}(t)\|^2 \\ &\leq (20 + 9(N_1 e^{M_1} + N_2 e^{M_2} + 2\epsilon) e^{N_2 e^{M_2} + \epsilon} \end{aligned}$$

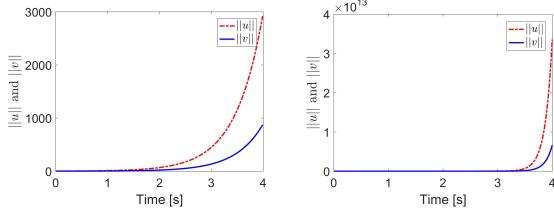


Fig. 4. Instability of the uncontrolled plant of  $u(x,t)$  and  $v(x,t)$  for given coefficients  $\lambda(x) = \Gamma x + 1$ ,  $\mu(x) = e^{\Gamma x} + 2$ ,  $\delta(x) = \Gamma(x + 1)$ ,  $\theta(x) = \Gamma(x + 1)$ ,  $\omega(x) = \Gamma(\cosh(x) + 1)$ ,  $q = \Gamma/3$ ,  $\Gamma = 2, 5$ .

$$+ 4N_1 e^{M_1} + 4N_2 e^{M_2} + 8\epsilon) \Psi_2(t). \quad (185)$$

Thus, we have completed the proof.  $\blacksquare$

With the help of Proposition 3 and 4 state we state following theorem.

**Theorem 4** For any  $\epsilon < \epsilon^*$  where

$$\epsilon^* := \frac{\sqrt{(B_u^2 + B_v^2 + B_{\hat{u}}^2 + B_{\hat{v}}^2)}}{\sqrt{S_2(\epsilon)\vartheta_5}} > 0, \quad (186)$$

and  $\|u(0)\|^2 + \|v(0)\|^2 + \|\hat{u}(0)\|^2 + \|\hat{v}(0)\|^2 \leq \zeta$ , where

$$\zeta := \frac{S_1(\epsilon)}{S_2(\epsilon)\vartheta_4(\epsilon)} \left( (B_u^2 + B_v^2 + B_{\hat{u}}^2 + B_{\hat{v}}^2) - S_2\vartheta_5\epsilon^2 \right) > 0, \quad (187)$$

the closed-loop system consisting of the NO approximation of the PDE feedback law (147) and the plant (1)–(4) and observer system (25)–(28) satisfy the semi-global practical exponential stability estimate,

$$\Phi_2(t) \leq \frac{S_2(\epsilon)}{S_1(\epsilon)} \vartheta_4(\epsilon) e^{-\vartheta_3(\epsilon)t} \Phi_2(0) + S_2\vartheta_5\epsilon^2, \quad \forall t \geq 0. \quad (188)$$

The estimate given by (188) is semi-global by permitting the radius  $\zeta$  of the initial condition ball in the  $L^2[0, 1]$  space to expand as the values of  $B_u, B_v, B_{\hat{u}}$ , and  $B_{\hat{v}}$  increase. Furthermore, the size of the training set as well as the number of nodes of the neural network are increasing functions of  $B_u, B_v, B_{\hat{u}}$ , and  $B_{\hat{v}}$ . Even though the stability is semi-global, the region of attraction  $\zeta$  defined in (187), remains considerably smaller than the magnitude of the samples associated with  $B_u, B_v, B_{\hat{u}}$ , and  $B_{\hat{v}}$  in the training set. Moreover, from (188), as  $t \rightarrow \infty$ , the residual value  $\Phi_2(t) \leq S_2\vartheta_5\epsilon^2$ , can be reduced to an arbitrarily small level by decreasing parameter  $\epsilon$ , and concurrently, by increasing both the training set size and the number of neural network nodes in accordance with the reduction of  $\epsilon$ .

## 6 Simulation

Our simulation is performed considering a  $2 \times 2$  linear hyperbolic system with  $\lambda(x) = \Gamma x + 1$ ,  $\mu(x) = e^{\Gamma x} + 2$ ,  $\delta(x) = \Gamma(x + 1)$ ,  $\theta(x) = \Gamma(x + 1)$ ,  $\omega(x) = \Gamma(\cosh(x) + 1)$ ,  $q = \Gamma/3$ , parameterized by  $\Gamma = \{2; 5\}$ . Under initial conditions  $u_0(x) = 1$ ,  $v_0(x) = \sin(x)$ , the open-loop system of the plant is unstable as shown in Figure 4. By iterating the functions  $\lambda(x)$ ,  $\mu(x)$ ,  $\delta(x)$ ,  $\theta(x)$ , and  $\omega(x)$  along the  $y$ -axis to generate a two-dimensional (2D) input for the  $\mathcal{K}$

network, the DeepONet is developed without modifying the grid structure. Similarly, the constant  $q$  is iterated along both  $x$  and  $y$  coordinates to generate additional 2D inputs for the  $\mathcal{K}$  network. In summary, this methodology results in six distinct 2D inputs for the network. Our approach capitalizes on this 2D structure by integrating a Convolutional Neural Network (CNN) into the branch network of the DeepONet. Exploiting a 2000 samples dataset, the model demonstrating the highest accuracy in data point classification is identified. Analytical and learned DeepONet kernels, namely  $k_1, k_2, m_1$ , and  $m_2$ , are depicted in Figures 5, 6, 7, and 8. These figures illustrate the kernels' behavior for two distinct values of  $\Gamma$ , specifically 2 and 5. During the training phase (refer to Fig. 10), the relative  $L^2$  errors for kernels  $k_1, k_2, m_1$ , and  $m_2$  were recorded as  $4.90 \times 10^{-5}$ ,  $3.48 \times 10^{-5}$ ,  $6.69 \times 10^{-5}$ , and  $2.61 \times 10^{-5}$ , respectively. The corresponding testing errors were  $5.32 \times 10^{-5}$ ,  $3.89 \times 10^{-5}$ ,  $7.34 \times 10^{-5}$ , and  $2.62 \times 10^{-5}$ .

Furthermore, we simulate the closed-loop system comprising the NO approximation of the PDE feedback law (147), the plant (1)–(4), and the observer system (25)–(27). Our control law is derived using a pre-designed learning network for the gain kernels, rather than directly from the inputs  $\lambda(x), \mu(x), \sigma(x), \omega(x), \theta(x), q, \hat{u}(x, t)$ , and  $\hat{v}(x, t)$ . These inputs are processed by neural operators from Section 4 to approximate kernel functions  $\hat{k}_i(x, \xi)$  and  $\hat{m}_i(x, \xi)$ ,  $i = 1, 2$ . These approximations are then linearly combined with observer estimates  $\hat{u}$  and  $\hat{v}$ . The final step uses a DeepONet layer to learn the mapping  $(\lambda, \mu, \sigma, \omega, \theta, q, \hat{u}, \hat{v}) \rightarrow \hat{U}$ . With 2000 samples, the model achieves an  $L^2$  error of  $5.46 \times 10^{-8}$  and a testing error of  $5.97 \times 10^{-8}$ , as shown in Figure 9. These simulations corroborate the closed-loop stability under output-feedback control law. That is shown in Figures 12 and 13. Moreover, Figure 14 displays the observer error in closed-loop solutions employing observer kernels  $\hat{m}_1(x, \xi)$  and  $\hat{m}_2(x, \xi)$ , along with the control law  $\hat{U}(t)$ .

## 7 Conclusion

In this paper, we demonstrate the potential application of DeepONet to a PDE backstepping boundary control law of  $2 \times 2$  linear coupled hyperbolic PDE system. Generally, these systems follow distributed dynamics and arise in modeling systems like water canals, traffic, power transmission, and oil drilling systems. In Section 1, we discussed major turning points in designing boundary controllers for broader classes of coupled hyperbolic PDEs, advocating for DeepONet's use as a proof-based Machine Learning method for PDE control. PDE Backstepping-based DeepONet combines data-driven methods with deductive Lyapunov arguments using reliable data to expedite gain function computation from a known plant's model. Key results include *Global Exponential Stability (GES)* for  $L^2$  initial data with approximated kernel functions and *Semi-global Practical Exponential Stability (SG-PES)* when the observer state is learned and fed to the controller.

## References

- [1] P. Goatin, The Aw-Rascle vehicular traffic flow model with phase transitions, *Mathematical and Computer Modelling* 44 (2006) 287–

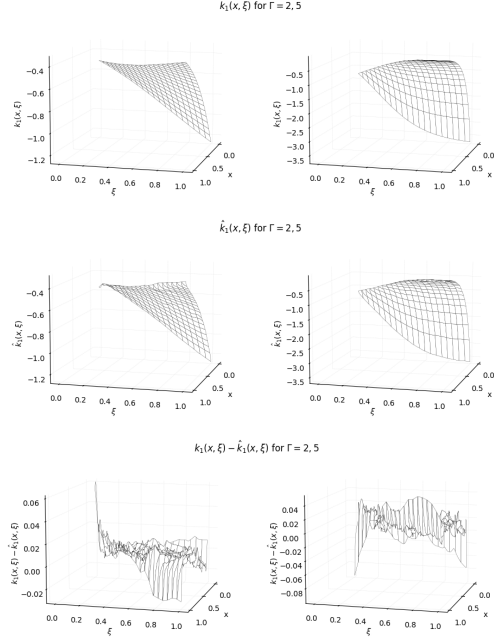


Fig. 5. The kernel of  $k_1(x, \xi)$ ,  $\hat{k}_1(x, \xi)$  and  $k_1(x, \xi) - \hat{k}_1(x, \xi)$ .

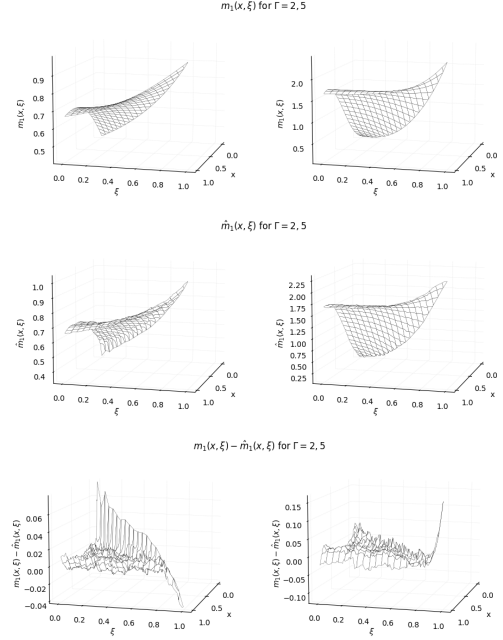


Fig. 7. The kernel of  $m_1(x, \xi)$ ,  $\hat{m}_1(x, \xi)$  and  $m_1(x, \xi) - \hat{m}_1(x, \xi)$ .

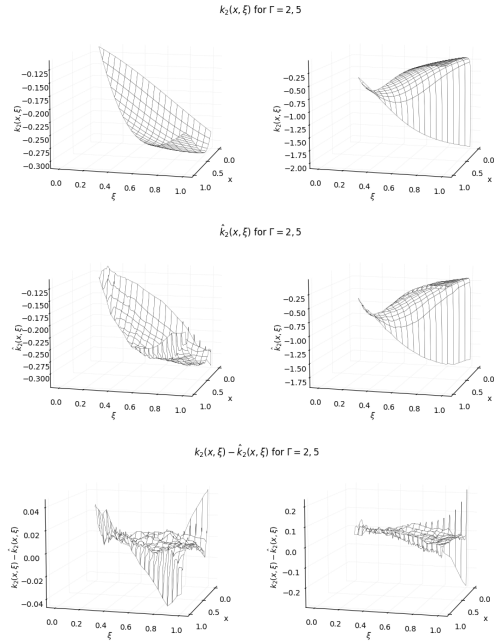


Fig. 6. The kernel of  $k_2(x, \xi)$ ,  $\hat{k}_2(x, \xi)$  and  $k_2(x, \xi) - \hat{k}_2(x, \xi)$ .

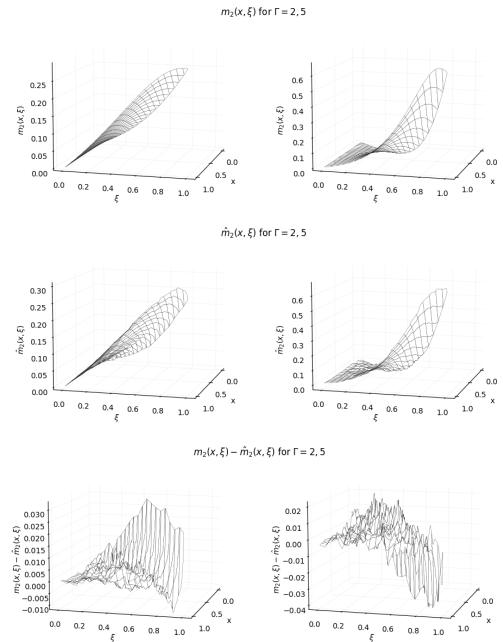


Fig. 8. The kernel of  $m_2(x, \xi)$ ,  $\hat{m}_2(x, \xi)$  and  $m_2(x, \xi) - \hat{m}_2(x, \xi)$ .

303.

- [2] H. Yu, M. Krstic, Traffic congestion control for aw-rascl-zhang model, *Automatica* 100 (2019) 38–51.
- [3] J. D. Halleux, C. Prieur, J. M. Coron, B. d'Andréa Novel, G. Bastin, Boundary feedback control in networks of open channels, *Automatica* 39 (8) (2003) 1365–1376.
- [4] A. Diagne, M. Diagne, S. Tang, M. Krstic, Backstepping stabilization of the linearized Saint-Venant-Exner model, *Automatica* 76 (2017) 345–354.
- [5] M. Diagne, S.-X. Tang, A. Diagne, M. Krstic, Control of shallow

- waves of two unmixed fluids by backstepping, *Annual Reviews in Control* 44 (2017) 211–225.
- [6] A. Diagne, G. Bastin, J.-M. Coron, Lyapunov exponential stability of 1-D linear hyperbolic systems of balance laws, *Automatica* 48 (1) (2012) 109–114.
- [7] C.-Z. Xu, G. Sallet, Exponential stability and transfer functions of processes governed by symmetric hyperbolic systems, *ESAIM: Control, Optimisation and Calculus of Variations* 7 (2002) 421–442.
- [8] O. M. Aamo, Leak detection, size estimation and localization in pipe flows, *IEEE Transactions on Automatic Control* 61 (1) (2016)

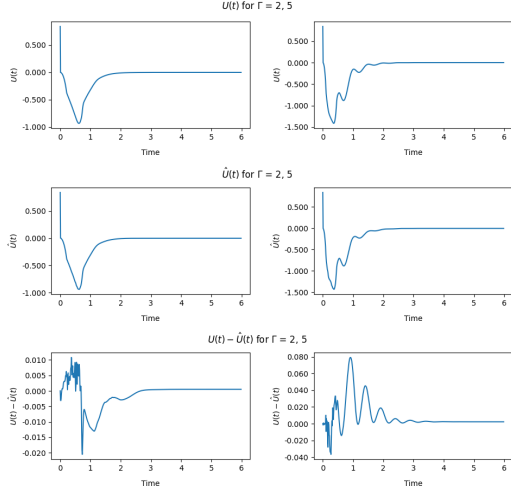


Fig. 9. Control law  $U$ ,  $\hat{U}$  and  $U - \hat{U}$ .

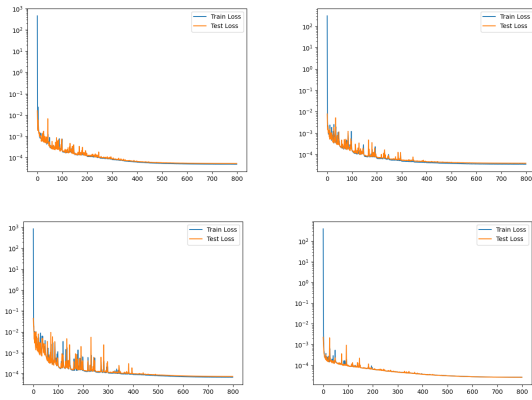


Fig. 10. The train and test loss for  $(\lambda(x), \mu(x), \omega(x), \sigma(x), \theta(x), q) \rightarrow (k_1(x, \xi), k_2(x, \xi), m_1(x, \xi), m_2(x, \xi))$ .

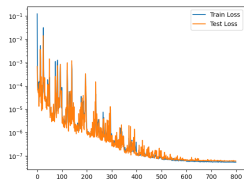


Fig. 11. The train and test loss for  $(\lambda(x), \mu(x), \omega(x), \sigma(x), \theta(x), q) \rightarrow U$ .

246–251.

- [9] R. Dáger, E. Zuazua, Wave propagation, observation and control in 1-D flexible multi-structures, Springer Science & Business Media, 2006.
- [10] M. Gugat, M. Dick, G. Leugering, Gas flow in fan-shaped networks: Classical solutions and feedback stabilization, *SIAM Journal on Control and Optimization* 49 (5) (2011) 2101–2117.
- [11] C. Curró, D. Fusco, N. Manganaro, A reduction procedure for generalized riemann problems with application to nonlinear transmission lines, *Journal of Physics A Mathematical & Theoretical* 44 (33) (2011) 335205.
- [12] J.-M. Coron, B. d’Andréa Novel, G. Bastin, A Lyapunov approach to

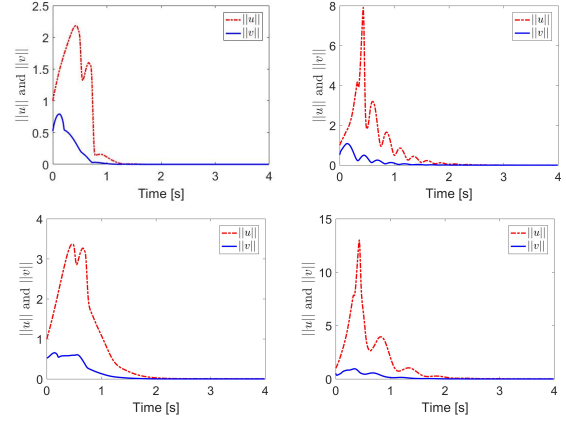


Fig. 12. **Upper row:** closed-loop solutions with the observer kernels  $m_1(x, \xi)$ ,  $m_2(x, \xi)$ , and the control law  $U(t)$ , respectively. **Lower row:** closed-loop solutions with the observer kernels  $\hat{m}_1(x, \xi)$ ,  $\hat{m}_2(x, \xi)$ , and control law  $\hat{U}(t)$ .

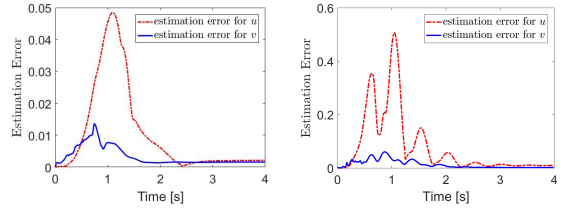


Fig. 13. Residual error induced by the DeepONet approximation.

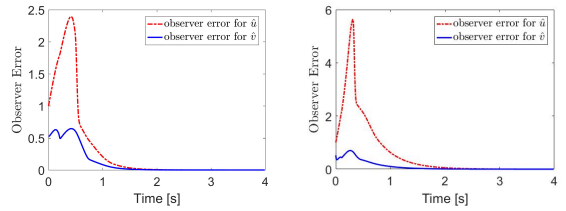


Fig. 14. Observer error with observer kernels  $\hat{m}_1(x, \xi)$  and  $\hat{m}_2(x, \xi)$  and control law  $\hat{U}(t)$ .

control irrigation canals modeled by saint-venant equations, in: 1999 European control conference (ECC), IEEE, 1999, pp. 3178–3183.

- [13] D. Bresch-Pietri, M. Krstic, Output-feedback adaptive control of a wave pde with boundary anti-damping, *Automatica* 50 (5) (2014) 1407–1415.
- [14] G. Bastin, J.-M. Coron, Further results on boundary feedback stabilisation of  $2 \times 2$  hyperbolic systems over a bounded interval, *IFAC Proceedings Volumes* 43 (14) (2010) 1081–1085.
- [15] G. Bastin, J.-M. Coron, On boundary feedback stabilization of non-uniform linear  $2 \times 2$  hyperbolic systems over a bounded interval, *Systems & Control Letters* 60 (11) (2011) 900–906.
- [16] R. Vazquez, M. Krstic, J.-M. Coron, Backstepping boundary stabilization and state estimation of a  $2 \times 2$  linear hyperbolic system, in: 2011 50th IEEE Conference on Decision and Control and European Control Conference, 2011, pp. 4937–4942.
- [17] R. Vazquez, M. Krstic, Bilateral boundary control of one-dimensional first- and second-order pdes using infinite-dimensional backstepping, in: 2016 IEEE 55th Conference on Decision and Control (CDC), IEEE, 2016, pp. 537–542.
- [18] J. Auriol, F. Di Meglio, Two-sided boundary stabilization of



- heterodirectional linear coupled hyperbolic pdes, *IEEE Transactions on Automatic Control* 63 (8) (2017) 2421–2436.
- [19] J. Wang, M. Diagne, Delay-adaptive boundary control of coupled hyperbolic PDE-ODE cascade systems, *IEEE Transactions on Automatic Control* doi:10.1109/TAC.2024.3399629.
- [20] I. Karafyllis, M. Kontorinaki, M. Krstic, Adaptive control by regulation-triggered batch least squares, *IEEE Transactions on Automatic Control* 65 (7) (2020) 2842–2855.
- [21] X. Litrico, V. Fromion, Boundary control of hyperbolic conservation laws using a frequency domain approach, *Automatica* 45 (3) (2009) 647–656.
- [22] T. S. Rabbani, F. Di Meglio, X. Litrico, A. M. Bayen, Feed-forward control of open channel flow using differential flatness, *IEEE Transactions on control systems technology* 18 (1) (2009) 213–221.
- [23] S. Tang, M. Krstic, Sliding mode control to the stabilization of a linear  $2 \times 2$  hyperbolic system with boundary input disturbance, in: 2014 American Control Conference, 2014, pp. 1027–1032.
- [24] V. D. S. Martins, M. Rodrigues, M. Diagne, A multi-model approach to saint-venant equations: A stability study by Imis, *International Journal of Applied Mathematics and Computer Science* 22 (3) (2012) 539–550.
- [25] F. Di Meglio, G.-O. Kaasa, N. Petit, V. Alstad, Model-based control of slugging: advances and challenges, *IFAC Proceedings Volumes* 45 (8) (2012) 109–115.
- [26] F. Di Meglio, R. Vazquez, M. Krstic, N. Petit, Backstepping stabilization of an underactuated  $3 \times 3$  linear hyperbolic system of fluid flow equations, in: 2012 American Control Conference (ACC), IEEE, 2012, pp. 3365–3370.
- [27] U. J. F. Aarsnes, F. Di Meglio, S. Evje, O. M. Aamo, Control-oriented drift-flux modeling of single and two-phase flow for drilling, in: *Dynamic Systems and Control Conference*, Vol. 46209, American Society of Mechanical Engineers, 2014, p. V003T37A003.
- [28] M. Burkhardt, H. Yu, M. Krstic, Stop-and-go suppression in two-class congested traffic, *Automatica* 125 (2021) 109381.
- [29] F. Di Meglio, R. Vazquez, M. Krstic, Stabilization of a system of  $n + 1$  coupled first-order hyperbolic linear PDEs with a single boundary input, *IEEE Transactions on Automatic Control* 58 (12) (2013) 3097–3111.
- [30] L. Hu, F. Di Meglio, R. Vazquez, M. Krstic, Control of homodirectional and general heterodirectional linear coupled hyperbolic PDEs, *IEEE Transactions on Automatic Control* 61 (11) (2016) 3301–3314.
- [31] L. Hu, R. Vazquez, F. D. Meglio, M. Krstic, Boundary exponential stabilization of 1-dimensional inhomogeneous quasi-linear hyperbolic systems, *SIAM Journal on Control and Optimization* 57 (2) (2019) 963–998.
- [32] J. Auriol, F. D. Meglio, Minimum time control of heterodirectional linear coupled hyperbolic PDEs, *Automatica* 71 (2015) 300–307.
- [33] H. Anfinsen, M. Diagne, O. M. Aamo, M. Krstic, An adaptive observer design for  $n + 1$  coupled linear hyperbolic PDEs based on swapping, *IEEE Transactions on Automatic Control* 61 (12) (2016) 3979–3990.
- [34] H. Anfinsen, M. Diagne, O. M. Aamo, M. Krstić, Estimation of boundary parameters in general heterodirectional linear hyperbolic systems, *Automatica: A journal of IFAC the International Federation of Automatic Control* (79) (2017) 185–197.
- [35] H. Anfinsen, O. M. Aamo, Adaptive control of hyperbolic PDEs, Springer, 2019.
- [36] J.-M. Coron, L. Hu, G. Olive, Finite-time boundary stabilization of general linear hyperbolic balance laws via fredholm backstepping transformation, *Automatica* 84 (2017) 95–100.
- [37] J.-M. Coron, L. Hu, G. Olive, P. Shang, Boundary stabilization in finite time of one-dimensional linear hyperbolic balance laws with coefficients depending on time and space, *Journal of Differential Equations* 271 (2021) 1109–1170.
- [38] I. Karafyllis, M. Krstic, Spill-free transfer and stabilization of viscous liquid, *IEEE Transactions on Automatic Control* 67 (9) (2022) 4585–4597.
- [39] I. Karafyllis, F. Vokos, M. Krstic, Output-feedback control of viscous liquid–tank system and its numerical approximation, *Automatica* 149 (2023) 110827.
- [40] L. Bhan, Y. Shi, M. Krstic, Neural operators for bypassing gain and control computations in PDE backstepping, *IEEE Transactions on Automatic Control* doi:10.1109/TAC.2023.3347499.
- [41] M. Krstic, L. Bhan, Y. Shi, Neural operators of backstepping controller and observer gain functions for reaction-diffusion PDEs, *Automatica* 164 (2024) 111649.
- [42] J. Qi, J. Zhang, M. Krstic, Neural operators for PDE backstepping control of first-order hyperbolic PIDE with recycle and delay, *Systems & Control Letters* 185 (2024) 105714.
- [43] Y. Zhang, R. Zhong, H. Yu, Neural operators for boundary stabilization of stop-and-go traffic, *arXiv preprint arXiv:2312.10374*.
- [44] M. Lamarque, L. Bhan, Y. Shi, M. Krstic, Adaptive neural-operator backstepping control of a benchmark hyperbolic PDE, *arXiv preprint arXiv:2401.07862* (submitted to *Automatica*).
- [45] M. Lamarque, L. Bhan, R. Vazquez, M. Krstic, Gain scheduling with a neural operator for a transport PDE with nonlinear recirculation, *arXiv preprint arXiv:2401.02511* (submitted to *IEEE Transactions on Automatic Control*).
- [46] L. Bhan, Y. Shi, I. Karafyllis, M. Krstic, J. B. Rawlings, Moving-horizon estimators for hyperbolic and parabolic PDEs in 1-D, *arXiv e-prints* (submitted to CDC) (2024) arXiv:2401.
- [47] S. Wang, M. Diagne, M. Krstic, Deep learning of delay-compensated backstepping for reaction-diffusion PDEs, *arXiv preprint arXiv:2308.10501* (submitted to *IEEE Transactions on Automatic Control*).
- [48] T. Chen, H. Chen, Universal approximation to nonlinear operators by neural networks with arbitrary activation functions and its application to dynamical systems, *IEEE Transactions on Neural Networks* 6 (4) (1995) 911–917.
- [49] L. Lu, P. Jin, G. Pang, Z. Zhang, G. E. Karniadakis, Learning nonlinear operators via deeponet based on the universal approximation theorem of operators, *Nature Machine Intelligence* 3 (3) (2021) 218–229.
- [50] L. Lu, P. Jin, G. E. Karniadakis, Deeponet: Learning nonlinear operators for identifying differential equations based on the universal approximation theorem of operators, *arXiv preprint arXiv:1910.03193*.
- [51] Z. Li, N. Kovachki, K. Azizzadenesheli, B. Liu, K. Bhattacharya, A. Stuart, A. Anandkumar, Fourier neural operator for parametric partial differential equations, *arXiv preprint arXiv:2010.08895*.
- [52] B. Deng, Y. Shin, L. Lu, Z. Zhang, G. E. Karniadakis, Approximation rates of deeponets for learning operators arising from advection-diffusion equations, *Neural Networks* 153 (2022) 411–426.